

# Polimery w Medycynie

## Polymers in Medicine

BIANNUAL ISSN: 0370-0747 e-ISSN: 2451-2699

[www.polimery.umed.wroc.pl](http://www.polimery.umed.wroc.pl)

2019, Vol. 49, No. 2 (July–December)

Ministry of Science and Higher Education – 9 pts.  
Index Copernicus (ICV) – 109.18 pts.



WROCLAW  
MEDICAL UNIVERSITY



# Polimery w Medycynie

## Polymers in Medicine

ISSN 0370-0747 (PRINT)

ISSN 2451-2699 (ONLINE)

[www.polimery.umed.wroc.pl](http://www.polimery.umed.wroc.pl)

**BIANNUAL**  
**2019, Vol. 49, No. 2**  
**(July–December)**

“Polymers in Medicine” is an independent, multidisciplinary forum to exchange scientific and clinical information, which publishes original papers (technical, analytical, experimental, clinical), preliminary reports and reviews regarding the use of polymers (natural and synthetic) and biomaterials in different specialties of medicine (biochemistry, clinical medicine, pharmacology, dentistry, implantology), biotechnology and veterinary science.

### Address of Editorial Office

Marcinkowskiego 2–6  
50-368 Wrocław, Poland  
Tel.: +48 71 784 11 33  
E-mail: [redakcja@umed.wroc.pl](mailto:redakcja@umed.wroc.pl)

### Publisher

Wrocław Medical University  
Wybrzeże L. Pasteura 1  
50-367 Wrocław, Poland

© Copyright by Wrocław Medical University,  
Wrocław 2019

Online edition is the original version of the journal

### Editor-in-Chief

Magdalena Krajewska  
Mariusz Kuształ

### Vice-Editor-in-Chief

Jerzy Gosk

### Editorial Board

Rajmund Adamiec  
Beata Dejak  
Bożena Karolewicz  
Witold Musiał

### Thematic Editors

Bożena Karolewicz  
(Multifunctional polymers in pharmaceutical technology and medical applications)  
Witold Musiał  
(Physicochemical evaluation of polymers used in pharmacy and medicine)  
Agnieszka Wojciechowska  
(Bioinorganic chemistry and coordination chemistry)  
Agnieszka Noszczyk-Nowak  
(Experimental research)

### International Advisory Board

Jennifer B. Dressman (Germany)  
Mirosława El Fray (Poland)  
Mukesh G. Gohel (India)  
Vipin B. Gupta (India)  
Anthony J. Hickey (USA)  
Jacek Kaczmarczyk (Poland)

### Secretary

Maciej Szymczak

Michał Nachajski  
Tadeusz Orłowski  
Lidia Usnarska-Zubkiewicz  
Włodzimierz Więtekiewicz

### Technical Editorship

Adam Barg, Marek Misiak,  
Paulina Kunicka

### Statistical Editors

Dorota Diakowska, Leszek Noga

### English Language Copy Editors

Jason Schock, Marcin Tereszewski,  
Sherill Howard Pocięcha

Agnieszka Noszczyk-Nowak (Poland)  
Paweł Reichert (Poland)  
Maciej Urban (Poland)  
Timothy S. Wiedmann (USA)  
Katarzyna Winnicka (Poland)  
Waldemar Wysokiński (USA)  
Samuel Yalkowsky (USA)

## Editorial Policy

During the review process, the Editorial Board conforms to the "Uniform Requirements for Manuscripts Submitted to Biomedical Journals: Writing and Editing for Biomedical Publication" approved by the International Committee of Medical Journal Editors (<http://www.icmje.org/>). Experimental studies must include a statement that the experimental protocol and informed consent procedure were in compliance with the Helsinki Convention and were approved by the ethics committee.

For more information visit the following page: <http://www.polimery.umed.wroc.pl>

Indexed in: OCLC, WorldCat, PBL, EBSCO, MEDLINE, Index Copernicus

This publication has been co-financed by the Ministry of Science and Higher Education

Typographic design: Monika Kołęda, Piotr Gil

Cover: Monika Kołęda

DTP: Wrocław Medical University Press

Printing and binding: EXDRUK

Circulation: 11 copies

## Contents

- 49 Olha Shpotyuk, Adam Ingram, Oleh Shpotyuk, Andrii Miskiv, Nina Smolar  
**PALS probing of photopolymerization shrinkage in densely packed acrylate-type dental restorative composites**
- 57 Bukola Christianah Adebayo-Tayo, Gbemisola Elisabeth Ogunleye, Omonike Ogbole  
**Biomedical application of greenly synthesized silver nanoparticles using the filtrate of *Trichoderma viride*: Anticancer and immunomodulatory potentials**
- 63 Harshita Agrawal, Rishabha Malviya, Pramod Kumar Sharma  
**Strategy to modulate the tumor microenvironment using nanoparticles**
- 67 Maciej Szymczak, Dorota Zielińska, Aleksandra Musiała  
**The use of different dialysis membranes in therapy of patients with multiple myeloma**
- 71 Beena Kumari, Aparna Khansili, Parmita Phougat, Manish Kumar  
**Comprehensive review of the role of acrylic acid derivative polymers in floating drug delivery system**



# PALS probing of photopolymerization shrinkage in densely packed acrylate-type dental restorative composites

Olha Shpotyuk<sup>1,A–F</sup>, Adam Ingram<sup>2,B,C,E,F</sup>, Oleh Shpotyuk<sup>3,A,C–F</sup>, Andrii Miskiv<sup>1,B,C,E,F</sup>, Nina Smolar<sup>1,A,C,E,F</sup>

<sup>1</sup> Department of Orthodontics, Danylo Halytsky Lviv National Medical University, Ukraine

<sup>2</sup> Department of Physics, Opole University of Technology, Poland

<sup>3</sup> Faculty of Science and Technology, Jan Dlugosz University of Czestochowa, Poland

A – research concept and design; B – collection and/or assembly of data; C – data analysis and interpretation;

D – writing the article; E – critical revision of the article; F – final approval of the article

Polymers in Medicine, ISSN 0370-0747 (print), ISSN 2451-2699 (online)

Polim Med. 2019;49(2):49–56

## Address for correspondence

Oleh Shpotyuk

E-mail: olehshpotyuk@yahoo.com

## Funding sources

None declared

## Conflict of interest

None declared

Received on December 23, 2019

Reviewed on January 28, 2020

Accepted on February 23, 2020

## Cite as

Shpotyuk O, Ingram A, Shpotyuk O, Miskiv A, Smolar N.

PALS probing of photopolymerization shrinkage in densely packed acrylate-type dental restorative composites.

Polim Med. 2019;49(2):49–56. doi:10.17219/pim/118394

## DOI

10.17219/pim/118394

## Copyright

© 2020 by Wrocław Medical University

This is an article distributed under the terms of the

Creative Commons Attribution 3.0 Unported (CC BY 3.0)

(<https://creativecommons.org/licenses/by/3.0/>)

## Abstract

**Background.** Using positron annihilation lifetime spectroscopy (PALS), microstructural changes in commercial dental restorative composites under light-curing polymerization were identified as a modification in mixed positron/Ps trapping, where the decay of positronium (Ps; the bound state of positrons and electrons) is caused by free-volume holes mainly in the polymer matrix, and positron trapping is defined by interfacial free-volume holes in a mixed filler–polymer environment. In loosely packed composites with a filler content of <70–75%, this process was related to the conversion of Ps-to-positron trapping.

**Objectives.** To disclose such peculiarities in densely packed composites using the example of the commercially available acrylate-based composite ESTA-3<sup>®</sup> (ESTA Ltd., Kiev, Ukraine), which boasts a polymerization volumetric shrinkage of only 1.5%.

**Material and methods.** ESTA-3<sup>®</sup> was used as a commercially available acrylate-based dental restorative composite. A fast-fast coincidence system of 230-ps resolution based on 2 photomultiplier tubes coupled to a BaF2 detector and ORTEC<sup>®</sup> electronics was used to register lifetime spectra in normal-measurement statistics. The raw PAL spectra were treated using x3-x2-CDA (coupling decomposition algorithm).

**Results.** The annihilation process in the densely packed dental restorative composites (DRCs), as exemplified by the commercially available acrylate-based composite ESTA-3<sup>®</sup>, is identified as mixed positron/Ps trapping, where o-Ps decay is caused by free-volume holes in the polymer matrix and interfacial filler–polymer regions, and free positron annihilation is defined by free-volume holes between filler particles. The most adequate model-independent estimation of the polymerization volumetric shrinkage can be done using averaged positron annihilation lifetime. A meaningful description of the transformations in Ps- and positron-trapping sites under light curing can be developed on the basis of a semiempirical model exploring x3-x2-CDA. There is a strong monolithization of agglomerated filler nanoparticles in these composites, caused by the photo-induced disappearing of positron traps at the cost of Ps-decaying holes.

**Conclusions.** Governing the polymerization void-evolution process in densely packed DRC ESTA-3<sup>®</sup> occurs mainly in the filler sub-system as positron-to-Ps trapping conversion, which is the reason for the low corresponding volumetric shrinkage.

**Key words:** acrylates, positron annihilation lifetime spectroscopy, dental restorative composites, light curing, photopolymerization

## Introduction

Acrylic-type polymers filled with inorganic particles/nanoparticles compose an important class of dental restorative composites (DRCs), which can be effectively polymerized under light curing.<sup>1–3</sup> The monomer chains characteristic of uncured DRC are cross-linked by intramolecular bonds forming a denser polymer–composite matrix, thus producing polymerization stress or volumetric shrinkage.<sup>3</sup>

In most dental restoratives with a moderate filler content (no more than 70–80%), which can be conditionally defined as loosely packed DRCs, the shrinkage-accompanied stress approaches 1.5–15 MPa and the volumetric shrinkage is in the range of 2–4%.<sup>3</sup> The commercially available DRCs Charisma<sup>®</sup> (Heraeus Kulzer GmbH, Hanau, Germany)<sup>4</sup> and Dipol<sup>®</sup> (Oksomat-AN Ltd., Kiev, Ukraine),<sup>5</sup> can be mentioned as typical examples of such restoratives. These DRCs composed of a monomer (bisphenol A-diglycidyl dimethacrylate and triethyleneglycol dimethacrylate) modified by glass filler particles of various sizes (typically, pyrogenic silica glass (SiO<sub>2</sub>)) to modify weight-packing densities, possess high volumetric shrinkage under light-curing polymerization (above ~2%).

Employing positron annihilation lifetime spectroscopy (PALS),<sup>6–10</sup> microstructural changes under polymerization were identified as a modification in mixed positron/Ps trapping, where positronium (Ps; the bound state of positron and electron decay) is caused by free-volume holes mainly in the polymer matrix, and positron trapping is defined by interfacial free-volume holes in the filler–polymer environment.<sup>11–15</sup> The PAL spectra of polymerized DRCs follow a multicomponent trapping model with respect to multichannel positron/Ps annihilation, with the number of physically realistic channels not being specifically defined. Most often, the PAL spectra of light-cured DRCs based on acrylate-type resins are reconstructed under partially constrained x4- or x3-term analysis.<sup>16–19</sup> However, the unconstrained x3-term decomposition seems more suitable for experimental PAL spectra governed by mixed positron/Ps trapping. Indeed, in such case, the process of Ps-to-positron trapping conversion can be successfully parameterized employing an x3-x2 coupling decomposition algorithm (CDA), validated for mixed positron/Ps-related annihilation in nanocomposites.<sup>20–23</sup>

At higher concentrations of filler (above ~80%) and corresponding lower proportions of resin in the mixture, the volumetric shrinkage is typically moderated to less than ~2%, since the reduced amount of resin shrinks less in a given volume of composite.<sup>3</sup> In these DRCs, the variations in particle size allow optimized particle distribution and adequate density, contributing to reduced shrinkage. This is a case of “low-shrinkage” DRCs, characterized as “densely monolithic” restoratives. This specificity in the inner composite make-up, with an increased proportion

of micro- (1–1.5 μm) and sub-micro-sized (~0.5 μm) glass or glass–ceramic particles and amorphous silica nano-sized particles (<40 nm) (above 80%) is thought to be associated with some changes in the underlying mechanism of free-volume modification under polymerization light-curing. In this paper, we attempt to study such peculiarities for densely packed DRCs using PALS with the commercially available acrylate-type composite ESTA-3<sup>®</sup> (ESTA Ltd., Kiev, Ukraine), which possesses a volumetric polymerization shrinkage of only 1.5%.<sup>24</sup>

## Material and methods

The specimens of ESTA-3<sup>®</sup> DRC were prepared by filling an inner volume of a disk-shaped plastic mold (6 mm in diameter and 2 mm in thickness). The bottom surface was covered with a polyethylene slice film, which was separated from the DRC along with the outer ring around the disk prior to PALS measurements. Some of the samples were polymerized by illuminating them with a curing dental wireless LED light source (LED.T4 SEASKY, Beijing, China), emitting light in the range of 420–480 nm with a power density output of ~900 mW/cm<sup>2</sup>. Under illumination, the guide tip of the light source was maintained just above the sample surface (at a distance of 7 mm) so that the light beam completely covered the sample surface. The batch of non-polymerized DRC samples was marked Dent 0, and further batches of photopolymerized samples were marked with numbers corresponding to the light curing duration in seconds (Dent 5, Dent 20, Dent 40, and Dent 60).

The methodology of the PALS studies was identical to that of our recent research.<sup>11–13</sup> The raw PAL spectra were registered with a fast-fast coincidence system of 230-ps resolution based on 2 Photonis XP2020/Q photomultipliers coupled to BaF<sub>2</sub> scintillator detectors (Scionix Holland B.V., Bunnik, the Netherlands) and ORTEC<sup>®</sup> electronics (ORTEC, Oak Ridge, USA). To ensure high reliability, each spectrum involved 1 M of elementary positron annihilation events, accumulated at a temperature of 22°C and a relative humidity of 35%,<sup>22</sup> using an Na isotope of ~50 kBq activity as a positron source sandwiched between 2 tested samples. The PAL spectra were processed using LT v. 9.0 program,<sup>25</sup> stabilizing the average positron lifetime,  $\tau_{av}^{\Sigma}$  as:

$$\tau_{av}^{\Sigma} = \sum_i I_i \tau_i, \quad (1)$$

where  $\tau_i$  and  $I_i$  denote positron lifetime and the intensity of the corresponding fitting components (the accuracy in lifetime  $\tau_i$  and intensity  $I_i$  was  $5 \pm 0.005$  ns and  $\pm 0.5\%$ , respectively).

The best fit of the collected PAL spectra for polymeric materials is achieved via mixed channels of trapping, which occurs from defect-related positron traps



and bound positron-electron states, i.e., positronium. This can be solved through the multi-component fitting of the PAL spectrum with 3 or 4 single exponentials under unconstrained (free-fitting components) or constrained (used most often for some fixed fitting parameters, such as the shortest positron lifetime, maintained close to 0.125 ns) decomposition procedures and normalized component intensities ( $i = 3$  or 4)

$$\sum_i I_i = 1. \quad (2)$$

Thus, the fitting covers realistic channels caused by positrons, which annihilate from delocalized states in defect-free bulk, and those trapped from spatially-extended free-volume defects (positron trapping) and Ps states through “pick-up” annihilation with an electron from the surrounding material (Ps decaying).

Ignoring the contribution from Ps decay, these spectra can be parameterized in terms of the canonical two-state simple trapping model (STM) with one kind of defect, parameters of defect-free lifetime  $t_b$ , the trapping rate in defects  $k_d$ , and the percentage of trapped positrons  $h$ .<sup>6,8,10</sup> The other channel is caused by annihilation from the Ps state as free particles or those interacting with electrons from the environment.<sup>7,9,10</sup> In a ground state, Ps exists as para-Ps (antiparallel spins), decaying intrinsically with 2 g-quanta and a 0.125-ns lifetime in a vacuum, and as ortho-Ps (parallel spins), decaying with 3 g-quanta and a 142-ns lifetime. In matter, since positron wave function overlaps with electron wave function outside, annihilation with such electrons having an antiparallel spin decreases their lifetime to 0.5–10 ns, resulting in 2 gamma-rays “pick-off” annihilation. Ps localized in free-volume holes provides an indication on their mean radii  $R$  in terms of  $\tau_3$  lifetime ( $I_3$  value correlates with the density of Ps sites) with respect to the Tao-Eldrup equation:

$$\tau_3 = 0.5 \cdot \left[ 1 - \frac{R}{R + \Delta R} + \frac{1}{2\pi} \cdot \sin\left(\frac{2\pi R}{R + \Delta R}\right) \right]^{-1} \quad (3)$$

where  $\Delta R = 0.166$  nm is the fitted empirical layer thickness.<sup>7</sup>

By fitting Equation 2 with the measured  $\tau_3$  values, radius  $R_3$  and the free volumes  $V_f$  can be determined, making it possible to calculate the fractional free volume  $f_v^3$  using the empirical constant,  $C = 0.0018 \text{ \AA}^{-3}$ .<sup>7</sup>

$$f_v^3 = C \cdot I_3 \cdot V_f \quad (4)$$

The PAL spectra in polymer–filler DRCs are known to be composed of mixed positron/Ps trapping channels.<sup>11–13</sup> If Ps-decay and positron-trapping sites are interconnected so that no changes occur in other channels, we can treat these spectra with x3-x2-CDA.<sup>20–23</sup> Within this approach, the experimental x3-term PAL spectra are transformed

into the generalized x2-term form for host (initial or non-polymerized) and modified (polymerized) DRCs. At this stage, we can simply resolve an additional second component ( $t_{int}$ ,  $I_{int}$ ) for a polymerized DRC with defect-related lifetime  $t_{int}$  and intensity  $I_{int}$ , as well as compensate component with the input in the first channel ( $t_n$ ,  $I_n$ ), assuming a reasonable condition of full inter-channel equilibrium. The interchangeable Ps/positron traps in the polymerized DRC can be parameterized accepting ( $t_n$ ,  $I_n$ ) and ( $t_{int}$ ,  $I_{int}$ ) as the first and second components, respectively, of the x2-term decomposed spectrum for some hypothetical medium which obeys the formalism of canonical two-state STM.<sup>6,8,10</sup> The defect-related lifetime  $t_{int}$  in this model reflects the appearing/disappearing traps depending on the positive/negative sign of both  $I_n$  and  $I_{int}$  intensities.<sup>20</sup>

In case of a stronger input from Ps decaying in the x3-term PAL spectrum, positron trapping can be defined in terms of the same STM, assuming 2 additional contributions from trapped positrons (the positron trapping component) and o-Ps (the o-Ps trapping component).<sup>12,26</sup> This model with 2 additional positron-trapping defects with  $\kappa_{d1}$  and  $\kappa_{d2}$  annihilation rates, defined as

$$\kappa_{d1} = I_2 \left( \frac{1}{\tau_1} - \frac{1}{\tau_2} \right) \quad (5)$$

and

$$\kappa_{d2} = I_3 \left( \frac{1}{\tau_1} - \frac{1}{\tau_3} \right), \quad (6)$$

allows a more correct estimation of bulk lifetime  $t_b$  related to annihilation from Bloch states<sup>20</sup>:

$$\tau_b = \left( \frac{I_1}{\tau_1} + \frac{I_2}{\tau_2} + \frac{I_3}{\tau_3} \right)^{-1}. \quad (7)$$

## Results and discussion

The PAL spectra of ESTA-3<sup>®</sup> DRC in the initial non-polymerized state (Dent 0) and after respective 60-second light exposure (Dent 60 sample) subjected to free x3-term decomposition are depicted in Fig. 1a and 1b, respectively. The narrow-restricted statistical scatter of variance tightly grouped around the horizontal axis at the bottom of Fig. 1 demonstrates that PALS measurements are adequately described within this decomposition procedure. The respective best-fit parameters, positron-trapping and Ps-decay modes are presented in Tables 1 and 2.

With respect to these data, the annihilation in all ESTA-3<sup>®</sup> DRC samples can be identified as mixed positron/Ps trapping, where the 3<sup>rd</sup> Ps decay component originates from free-volume holes in the polymer matrix,

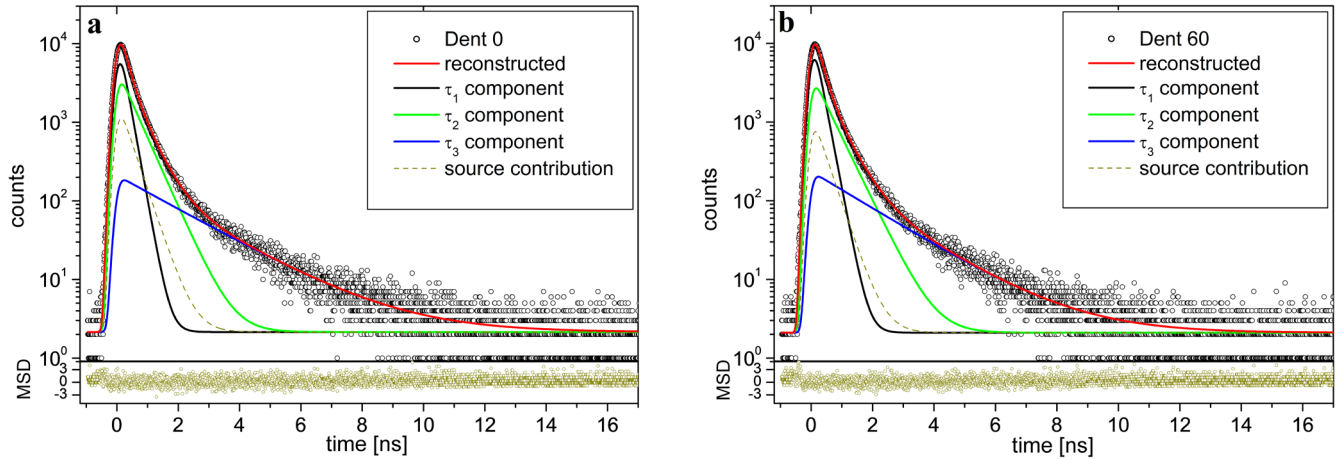


**Fig. 1.** Positron annihilation lifetime (PAL) spectra of non-polymerized dental restorative composite (DRC) Dent 0 (a) and polymerized DRC Dent 60 (b), reconstructed from unconstrained x3-fitting at the general background of source contribution; the bottom insets show the statistical scatter of variance – mean square deviation (MSD).

**Table 1.** The best-fit PAL spectra parameters for ESTA-3<sup>®</sup> DRC determined with an unconstrained x3-term decomposition procedure

DRC exposure [s]	[FIT-1]	$\tau_1$ [ns]	$\tau_2$ [ns]	$\tau_3$ [ns]	$I_2$ [a.u.]	$I_3$ [a.u.]	$\tau_{avg}$ [ns]
Dent 0	0.01	0.202	0.501	2.030	0.430	0.075	0.468
Dent 5	0.07	0.204	0.512	1.924	0.410	0.077	0.465
Dent 20	0.04	0.208	0.518	1.813	0.410	0.080	0.462
Dent 40	0.06	0.208	0.521	1.779	0.410	0.081	0.463
Dent 60	0.01	0.211	0.529	1.768	0.390	0.080	0.460

**Table 2.** The best-fit PAL spectra parameters for ESTA-3<sup>®</sup> DRC determined with an unconstrained x-term decomposition procedure

DRC exposure [s]	e <sup>+</sup> -trapping modes						Ps-decaying modes		
	$\tau_{avg}^{tr}$ [ns]	$\tau_b$ [ns]	$K_d$ [ns <sup>-1</sup> ]	$\tau_2 - \tau_b$ [ns]	$\tau_2/\tau_b$ [a.u.]	$\eta$ [a.u.]	$R_3$ [nm]	$V_f$ [10 <sup>-3</sup> nm <sup>3</sup> ]	$f_v^3$ [%]
Dent 0	0.340	0.279	1.36	0.222	1.80	0.27	0.291	103	1.40
Dent 5	0.342	0.280	1.32	0.232	1.83	0.27	0.280	92	1.28
Dent 20	0.345	0.283	1.28	0.235	1.83	0.27	0.270	82	1.18
Dent 40	0.346	0.283	1.27	0.238	1.84	0.26	0.267	80	1.16
Dent 60	0.347	0.284	1.21	0.245	1.86	0.26	0.266	80	1.12

and the 2<sup>nd</sup> component is defined by positron traps located mainly in the filler.<sup>12</sup> A comparative presentation of the x3-term-decomposed PAL spectra for the non-polymerized Dent 0 and the polymerized Dent 60 samples in Fig. 2 speaks in favor of a decrease in average positron lifetime  $\tau_{avg}$  under polymerization due to a shorter “tail” in the histogram of positron annihilation events connected with Ps decay. With longer photopolymerization, the  $\tau_3$  lifetime shows a distinct 13% decrease (from 2.030 to 1.788 ns under 60-second exposure), while  $I_3$  intensity clearly grows by 7% (Table 1). The radii of Ps-decay holes in these DRCs estimated in a spherical approximation using Equation 2 show a monotonically decreasing trend from 0.291 nm (for Dent 0) to 0.266 nm (for Dent 60). The sharp decrease in  $\tau_3$  results in systematic decaying in the fractional free volumes  $f_v^3$  was calculated with Equation 4.

In contrast, the changes observed in the 2<sup>nd</sup> component are opposite to light-curing duration, the  $\tau_2$  lifetime demonstrating an increasing trend (from 0.501 ns for Dent 0 to 0.529 ns for Dent 60) and the respective  $I_2$  intensity decreasing (Table 1). Under essential input from Ps decay, as in the case of ESTA-3<sup>®</sup> DRC, parameterization of this channel in terms of a two-state STM is meaningless. Nevertheless, given the obvious reverse trend in both intensities  $I_3$  and  $I_1$  with respect to  $I_2$  (Table 1), these changes in the PAL spectra with increased light curing duration can be attributed to preferential modification in the probability of Ps formation,<sup>27</sup> thus favoring positron-to-Ps trapping conversion in polymerized ESTA-3<sup>®</sup> DRC described by x3-x2-CDA.<sup>20–23</sup>

The more realistic values of defect-free bulk positron lifetime  $t_b$  related to positron annihilation from Bloch states can be extracted from STM assuming additional positron-trapping inputs from both trapped positrons

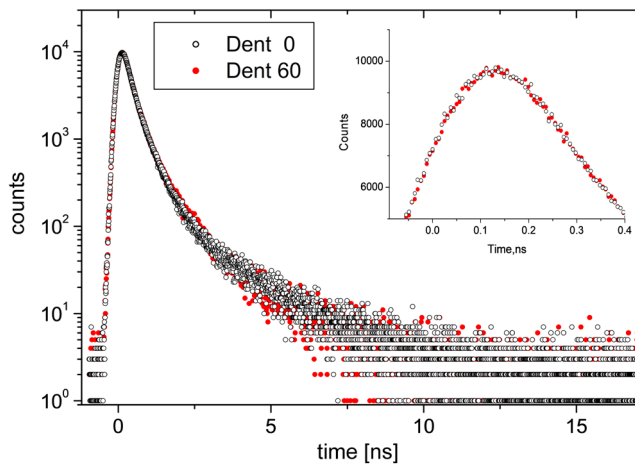


Fig. 2. PAL spectra of non-polymerized DRC Dent 0 (open circles) compared with the polymerized DRC Dent 60 (full red circles), reconstructed from unconstrained x3-term decomposition (the inset shows a comparison of annihilation events accumulated in a peak)

and decayed o-Ps states (with the positron lifetimes  $\tau_2$  and  $\tau_3$  given in Table 1). This  $t_b$  value, estimated by Equation 7, approaches 0.30 ns (Table 4) and is nearly 15% longer than that extracted from the constraint-free x3-term decomposition (Table 2). It is clear from Table 3 that light-curing polymerization leads to a decrease in the rate of “purely positron” trapping  $k_{d1}$  (by nearly 16%) compared to the trapping rate of “o-Ps decaying” channel  $k_{d2}$ , which remains essentially the same.

The PAL spectra of ESTA-3<sup>®</sup> DRC in the initial state (Dent 0) and after 60 s of exposure (Dent 60) subjected to partially constrained x4-term decomposition and as-

Table 4. PAL trapping modes for ESTA-3<sup>®</sup> DRC within an unconstrained x3-term decomposition, assuming 2 additional positron-trapping defect states

DRC exposure [s]	$\tau_{avg}^{tr}$ [ns]	$\tau_b$ [ns]	$K_{d1}$ [ns <sup>-1</sup> ]	$K_{d2}$ [ns <sup>-1</sup> ]
Dent 0	0.468	0.297	1.27	0.33
Dent 60	0.460	0.304	1.11	0.33

suming  $\tau_1 = 0.125$  ns (i.e., fixed at p-Ps self-annihilation lifetime) are depicted in Fig. 3a and 3b, respectively; the best-fit parameters, positron-trapping and Ps-decay modes under this decomposition procedure are presented in Table 4. Such an analysis was shown to be reasonable for polymer–matrix composites, where the basic polymer shows bifurcation in o-Ps lifetimes, as in, for example, some semicrystalline polymers.<sup>28,29</sup> In this case, the 4<sup>th</sup> component is attributed to o-Ps pick-off annihilation in holes of amorphous structures ( $\tau_4 \approx 2–4$  ns), and the 3<sup>rd</sup> component is ascribed to o-Ps pick-off annihilation in interstitial free-volume voids of crystalline phase ( $\tau_3 \approx 1$  ns).

Still, this is not the current case, since the polymer matrix of ESTA-3<sup>®</sup> DRC based on bisphenol A polycarbonates is solely characterized by x3-term PAL spectra, where the only long-lived component comes from o-Ps decay.<sup>30–32</sup> Simple physical mixing in the 2<sup>nd</sup> component of the x4-term-decomposed PAL spectra originating from interfacial holes and other free-volume defects in a solid/polymer phase cannot be excluded to separate realistic physical channels. Therefore, this analysis provides an invalid parameterization of the 2<sup>nd</sup> component as an artifact of inadequately

Table 3. PAL spectra fitting parameters for ESTA-3<sup>®</sup> DRC within a partially constrained x4-term decomposition ( $\tau_1 = 0.125$  ns)

DRC exposure [s]	[FIT-1]	PAL spectra fitting parameters						$\tau_{avg}$ ns
		$\tau_2$ [ns]	$\tau_3$ [ns]	$\tau_4$ [ns]	$I_2$ a.u.	$I_3$ a.u.	$I_4$ a.u.	
Dent 0	0.01	0.244	0.539	2.070	0.45	0.356	0.072	0.465
Dent 60	0.01	0.227	0.547	1.788	0.51	0.363	0.077	0.459

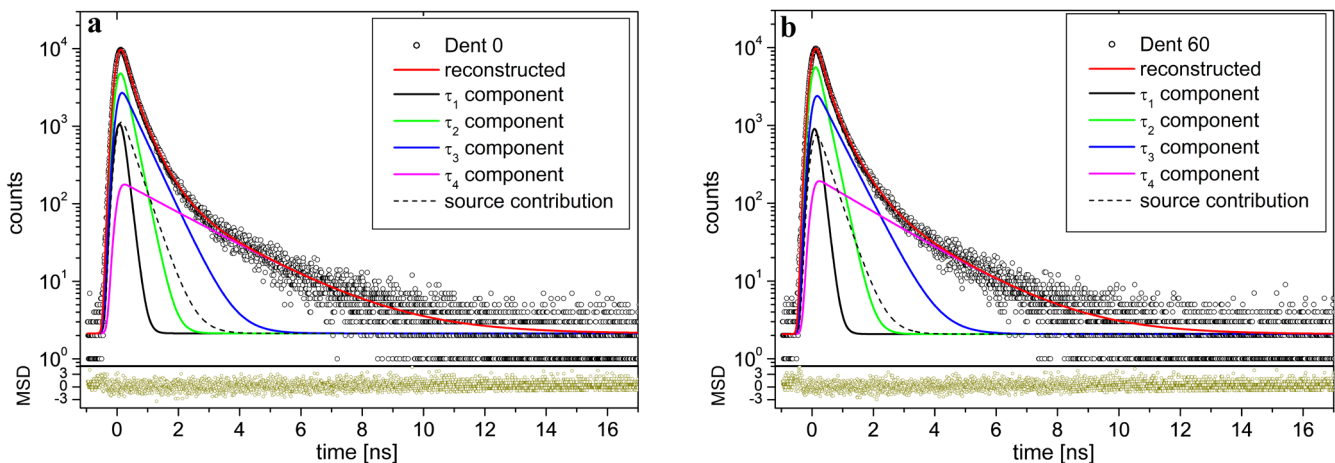


Fig. 3. PAL spectra of non-polymerized DRC Dent 0 (a) and polymerized DRC Dent 60 (b), reconstructed from partially constrained x4-fitting under fixed  $\tau_1 = 0.125$  ns at the general background of source contribution; the bottom insets show the statistical scatter of variance - mean square deviation (MSD)

fitting  $\times 4$ . In case of multiple o-Ps decays of the same origin, this component can be easily replaced by apparent lifetime, which is a mean value averaged over all o-Ps components with corresponding intensities.<sup>33</sup> It can clearly be seen from Table 4 that changes in the 3<sup>rd</sup> component can indeed be ignored, thus transforming the partially constrained (with  $\tau_1 = 0.125$  ns)  $\times 4$ -term-decomposed PAL spectra into free  $\times 3$ -term-decomposed ones (Table 1).

It is known that when free-volume voids are mutually inter-transformed under trapping conversion, the  $\times 3$ -term-decomposed PAL spectra can be treated using the  $\times 3$ - $\times 2$ -CDA for uncured DRCs with a light-cured one (in this case, both  $I_n$  and  $I_{int}$  are positive); the results of such treatment for the current DRC are presented in Table 5. This analysis shows that positron trapping sites like triple junctions, mainly between agglomerated filler particles with character-defect-specific lifetimes of  $\sim 0.34$ – $0.36$  ns, disappear under light curing in favor of o-Ps-decaying holes with lifetimes of  $\sim 1.7$ – $1.8$  ns and corresponding to decreased free volumes in the polymer matrix. These disappearing positron traps are like triple junctions between agglomerated filler particles, located in filler environment, as it follows from the low  $t_B$  in Table 5 — with values typical of nanosized glassy particles of silica or zirconia.<sup>34</sup> In other words, agglomerated filler particles/nanoparticles are strongly monolithized under light-curing polymerization in these DRCs, caused by photo-induced cross-linking of structural chains in the polymer matrix.

In Table 5,  $\times 3$ - $\times 2$ -CDA data calculated for Dent 40 in comparison with Dent 60 is also presented, allowing a comparison of the initial (0–20 s) and final (40–60 s) stages of light-curing polymerization. It is noteworthy that these stages differ only by defect-specific  $t_{int}$  and defect-free  $t_B$  positron lifetimes, meaning that under initial exposure the larger free-volume positron traps (with 0.358-ns lifetimes) disappear in looser filler packing (because  $t_B = 0.208$  ns), while the finest free-volume voids (with 0.312-ns lifetimes) disappear under final exposure in a denser filler environment (because  $t_B = 0.182$  ns). This feature explains the lower degree of volumetric shrinkage under polymerization in the densely monolithic ESTA-3<sup>®</sup> DRC as compared with other available loosely monolithic DRCs, particularly, the previously studied DRCs Charisma<sup>®</sup> and Dipol<sup>®</sup>.<sup>11–13</sup>

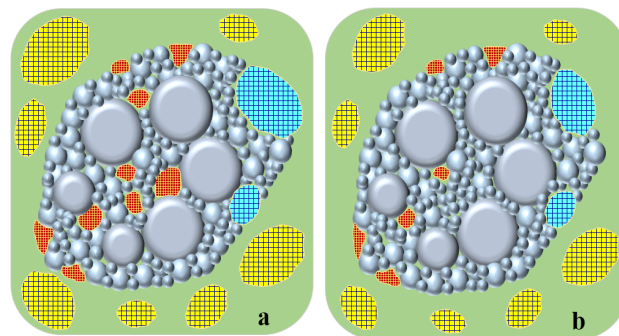


Fig. 4. Schematic view of the fragmentation of free-volume Ps and positron traps in light-cured DRC: a) microstructure fragment of agglomerated filler particles (grey) in a non-polymerized DRC matrix (green), containing an o-Ps-trapping void located in the interfacial filler–polymer region (blue-cross-dashed line), o-Ps-trapping holes mainly in the polymer matrix (yellow-cross-dashed line) and positron trapping sites in the filler matrix (red-cross-dashed line); b) the same agglomerate of filler particles in a polymerized DRC matrix (an o-Ps-trapping void in the interfacial filler–polymer region disappears, giving rise to more contracted o-Ps-trapping voids in the surrounding polymer matrix and reduced trapping sites within the agglomerated filler particles)

The results described above lead to a complete protocol of light-curing polymerization for ESTA-3 DRC (Fig. 4). In the initial non-polymerized state (Fig. 4a), these densely packed DRCs are filled in positron traps located preferentially in the filler sub-system (Fig. 4a, red-cross-dashed lines), as well as Ps-decaying voids placed in the interfacial filler–polymer region (blue-cross-dashed lines) and the polymer matrix (yellow-cross-dashed lines). Light-curing polymerization causes cross-linking of the latter, thus resulting in the fragmentation of the Ps decay sites in the polymer matrix (Fig. 4b, yellow-cross-dashed lines). The o-Ps-trapping voids in the interfacial filler–polymer region (blue-cross-dashed lines, Fig. 4b) are also reduced in size, and some of them disappear, giving rise to more tight contact between the outermost polymer surface, completely covering agglomerated filler particles. Under further progressive polymerization, strong contraction stress suppresses the agglomerate of filler particles, reducing the size and number of intrinsic free-volume positron traps (red-cross-dashed lines in Fig. 4b). Thus, the most substantial changes in free volume mainly take place in the filler sub-system, which is a reason for the low value of the corresponding volumetric shrinkage of this DRC.

Table 5. Positron-trapping modes for non-polymerized Dent 0 sample, calculated with respect to light-cured ESTA-3<sup>®</sup> DRC samples employing  $\times 3$ - $\times 2$  coupling decomposition algorithm (CDA)

DRC system	I component		II component		e <sup>+</sup> -trapping modes				
	$\tau_n$ [ns]	$I_n$ [a.u.]	$\tau_{int}$ [ns]	$I_{int}$ [a.u.]	$\tau_{av}$ [ns]	$\tau_B$ [ns]	$K_d$ [ns <sup>-1</sup> ]	$\tau_{int}-\tau_B$ [ns]	$\tau_{int}/\tau_B$ [a.u.]
Dent 0 – Dent 5	0.173	0.029	0.358	0.031	0.268	0.236	1.539	0.122	1.52
Dent 0 – Dent 20	0.150	0.049	0.358	0.046	0.250	0.208	1.859	0.150	1.72
Dent 0 – Dent 40	0.153	0.052	0.350	0.050	0.250	0.211	1.805	0.139	1.66
Dent 0 – Dent 60	0.149	0.067	0.342	0.064	0.243	0.205	1.862	0.137	1.67
Dent 40 – Dent 60	0.133	0.017	0.312	0.015	0.217	0.182	2.027	0.130	1.71

Finally, under the contribution of mixed positron/Ps trapping channels in the overall annihilation process in composites, one of the best estimations of volumetric polymerization shrinkage, whichever the spectra-reconstruction algorithms, is related to the average lifetime defined as mass center of the registered PAL spectrum defined by Equation 1. As follows from Table 1, light curing results in a decrease in  $t_{avg}$  from 0.468 ns for non-polymerized DRCs to 0.460 ns for completely polymerized DRCs. The relative change (1.7%) happens to be surprisingly close to the polymerization volumetric shrinkage of 1.5%, which is characteristic of ESTA-3<sup>®</sup>.<sup>24</sup>


## Conclusions


Some peculiarities of volumetric shrinkage under photopolymerization are studied using PALS in a densely packed DRC — the commercially available acrylate-based composite ESTA-3<sup>®</sup>. The PAL spectra are reconstructed from unconstrained x3-term and partially constrained x4-term fitting routes assuming the shortest lifetime fixed at a theoretical value of intrinsic para-Ps self-annihilation (0.125 ns), and a simple trapping model assuming additional inputs from trapped positrons and decayed o-Ps states.

With respect to the data obtained, the annihilation in these DRCs is identified as mixed positron/Ps trapping, where the contribution from o-Ps decay is caused by free-volume holes in the polymer matrix and interfacial filler–polymer voids, and the free positron annihilation is defined by free-volume holes between the filler particles. The most adequate model-independent estimation of photopolymerization volumetric shrinkage is achieved using the average positron annihilation lifetime. A meaningful description of the transformations between Ps- and positron-trapping sites under light curing was developed on the basis of a semi-empirical model exploring the x3-x2-CDA. Under polymerization, the most substantial changes in free volume occur mainly in the filler sub-system, which is the reason for the low value of corresponding volumetric shrinkage of this DRC.

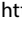
### ORCID iDs

Olha Shpotyuk  <https://orcid.org/0000-0002-9572-1817>

Adam Ingram  <https://orcid.org/0000-0002-8424-2298>

Oleh Shpotyuk  <https://orcid.org/0000-0002-2455-1857>

Andrii Miskiv  <https://orcid.org/0000-0001-7762-5867>

Nina Smolar  <https://orcid.org/0000-0001-8593-5435>

### References

- Bland MH, Peppas NA. Photopolymerized multifunctional (meth) acrylates as model polymers for dental application. *Biomaterials*. 1996;17:1109–1114. doi:10.1016/0142-9612(96)85912-6
- Cramer NB, Stansbury JW, Bowman CN. Recent advantages and developments in composite dental restorative materials. *J Dent Res*. 2011;90:402–416. doi:10.1177/0022034510381263
- Miletic V (ed). *Dental Composite Materials for Direct Restorations*. Cham, Switzerland: Springer Nature; 2018:319. doi:10.1007/978-3-319-60961-4
- Charisma<sup>®</sup>. Scientific Information. Heraeus Kulzer GmbH, Hanau, Germany. <https://www.pantelides-dental.gr/userfiles/files/CharismaScientificInformation.pdf>. Accessed on April 24, 2020.
- Dipol<sup>®</sup>. Composite Universal. Instruction on using Dipol materials. Oksomat-AN, Ukraine Dental Products, 2016;6-7. [www.oksomat-an.com](http://www.oksomat-an.com). Accessed on April 24, 2020.
- Krause-Rehberg R, Leipner HS. *Positron Annihilation in Semiconductors: Defect Studies*. Heidelberg, Germany: Springer 1999:383.
- Jean YC. Positron annihilation spectroscopy for chemical analysis: A novel probe for microstructural analysis of polymers. *Microchem J*. 1990;42:72–102. doi:10.1016/0026-265X(90)90027-3
- Shpotyuk O, Filipecki J. Free Volume in Vitreous Chalcogenide Semiconductors: Possibilities of Positron Annihilation Lifetime Study. Czestochowa, Poland: WSP; 2003:114.
- Jean YC, Van Horn JD, Hung WS, Lee KR. Perspective of positron annihilation spectroscopy in polymers. *Macromolecules*. 2013;46:7133–7145. doi:10.1021/ma401309x
- Tuomisto F, Makkonen I. Defect identification in semiconductors with positron annihilation: Experiment and theory. *Rev Mod Phys*. 2013;85:1583–1631. doi:10.1103/RevModPhys.85.1583
- Shpotyuk O, Ingram A, Shpotyuk O. Free volume structure of acrylic-type dental nanocomposites tested with annihilating positrons. *Nanoscale Res Lett*. 2016;11:528-1–528-6. doi:10.1186/s11671-016-1751-8
- Shpotyuk O, Ingram A, Shpotyuk O, Bezvushko E. Light-cured dimethacrylate dental restorative composites under a prism of annihilating positrons. *Polim Med*. 2017;47:91–100. doi:10.17219/pim/81450
- Shpotyuk O, Adamiak S, Bezvushko E, et al. Light-curing volumetric shrinkage in dimethacrylate-based dental composites by nanoindentation and PAL study. *Nanoscale Res Lett*. 2017;12:75-1–75-6. doi: 10.1186/s11671-017-1845-y
- Chakraverty S, Mitra S, Mandal K, Nambissan PMG, Chattopadhyay S. Positron annihilation studies of some anomalous features of NiFe<sub>2</sub>O<sub>4</sub> nanocrystals grown in SiO<sub>2</sub>. *Phys Rev B*. 2005;71:024115-1–8. doi:10.1103/PhysRevB.71.024115
- Mitra S, Mandal K, Sinha S, Nambissan PMG, Kumar S. Size and temperature dependent cationic redistribution in NiFe<sub>2</sub>O<sub>4</sub> (SiO<sub>2</sub>) nanocomposites: Positron annihilation and Mössbauer studies. *J Phys D: Appl Phys*. 2006;39:4228–4235. doi:10.1088/0022-3727/39/19/016
- Kleczevska J, Bieliński DM, Dryzek E, Piatkowska A. Application of positron annihilation lifetime spectroscopy in studies of dental composites based on dimethacrylate resins. In: Pielichowski K, ed. *Modern Polymeric Materials For Environmental Application*, 4(1). Krakow, Poland: TEZA; 2010:143-150.
- Kleczevska J, Bieliński DM, Ranganathan N, Sokolowski J. Characterization of light-cured dental composites. In: Ranganathan N, ed. *Materials Characterization. Modern Methods and Applications*. Boca Raton, USA: CRC Press; 2016:117–148.
- Shirazinia M, Mehmandoust-Khajen-Dad A, Dehghani V, Mehmandoust-Khajen-Dad J, Khaghani M. The effect of curing light intensity on free volume size in some dental composites. *Polim Med*. 2016;46:129–133. doi:10.17219/pim/68647
- Svajdlenkova H, Sausa O, Peer G, Gorsche C. In situ investigation of the kinetics and microstructure during photopolymerization by positron annihilation technique and NIR-photorheology. *RSC Adv*. 2018;8:37085-1–7. doi:10.1039/C8RA07578F
- Shpotyuk O, Filipecki J, Ingram A, et al. Positronics of subnanometer atomistic imperfections in solids as a high-informative structure characterization tool. *Nanoscale Res Lett*. 2015;10:77-1–5. doi:10.1186/s11671-015-0764-z
- Shpotyuk O, Ingram A, Filipecki J, Bujňáková Z, Baláz P. Positron annihilation lifetime study of atomic imperfections in nanostructured solids: On the parameterized trapping in wet-milled arsenic sulfides As<sub>4</sub>S<sub>4</sub>. *Phys Stat Solidi B*. 2016;253:1054–1059. doi:10.1002/pssb.201552560
- Shpotyuk Ya, Cebulski J, Ingram A, Shpotyuk O. Mathematical modelling of elementary trapping-reduction processes in positron annihilation lifetime spectroscopy: Methodology of Ps-to-positron trapping conversion. *J Phys (Conf Ser)*. 2017;936:012049-1–012049-4. doi:10.1088/1742-6596/936/1/012049
- Shpotyuk O, Ingram A, Shpotyuk Y. Free-volume characterization of nanostructured substances by positron annihilation lifetime spectroscopy. *Nucl Instr Meth Phys Res B*. 2018;416:102–109. doi:10.1016/j.nimb.2017.12.012

24. ЭСТА-3®. Dental photocured material for tooth filling. ЭСТА-3 microhybrid. Instruction on using. Ukraine, Kiev (2016). <http://www.esta-dental.kiev.ua/downloads/download/esta-3.pdf>. Accessed December 23, 2019.
25. Kansy J. Microcomputer program for analysis of positron annihilation lifetime spectra. *Nucl Instr Meth Phys Res A*. 1996;374:235–244. doi:10.1016/0168-9002(96)00075-7
26. Liu M, Kitai AH, Mascher P. Point defects and luminescence centers in zinc oxide and zinc oxide doped with manganese. *J Luminescence*. 1992;54:35–42. doi:10.1016/0022-2313(92)90047-D
27. Vijay YK, Wate S, Awasthi DK, Das D, Ghughre S. Ion induced effects in polymers. *Indian J Eng Mater Sci*. 2000;7:375–377.
28. Dannefaer S, Bretagnon T, Kerr D. Vacancy-type defects in crystalline and amorphous SiO<sub>2</sub>. *J Appl Phys*. 1993;7:884–890. doi:10.1063/1.354882
29. Dlubek G, Clarke AP, Fretwell HM, Dugdale SB, Alam MA. Positron lifetime studies of free volume hole size distribution in glassy polycarbonate and polystyrene. *Phys Status Solidi A*. 1996;157:351–364. doi:10.1002/pssa.2211570218
30. Dlubek G, Saarinen K, Fretwell HM. Positron states in polyethylene and polytetrafluoroethylene: A positron lifetime and Doppler-broadening study. *Nucl Instr Meth Phys Res B*. 1998;142:139–155. doi:10.1016/S0168-583X(98)00261-4
31. Pfeifer CS, Shelton ZR, Braga RR, Windmoller D, Machalo JC, Stansbury JW. Characterization of dimethacrylate polymeric networks: A study of the crosslinked structure formed by monomers used in dental composites. *Eur Polym J*. 2011;47:162–170. doi:10.1016/j.eurpolymj.2010.11.007
32. Kluin JE, Yu Z, Vleeshouwers S, McGervey JD, Jamieson AM, Simha R. Temperature and time dependence of free volume in bisphenol A polycarbonates studied by positron lifetime spectroscopy. *Macromolecules*. 1992;25:5089–5093. doi:10.1021/ma00045a040
33. Kluin JE, Yu Z, Vleeshouwers S, et al. Ortho-positronium lifetime studies of free volume in polycarbonates of different structures: Influence of hole size distribution. *Macromolecules*. 1993;26:1853–1861. doi:10.1021/ma00060a010
34. Ingram A. Atomic-deficient nanostructurization in water-sorption alumomagnesium spinel ceramics MgAl<sub>2</sub>O<sub>4</sub>. *Appl Nanosci*. 2019;9:731–735. doi:10.1007/s13204-018-0696-x

# Biomedical application of greenly synthesized silver nanoparticles using the filtrate of *Trichoderma viride*: Anticancer and immunomodulatory potentials

Bukola Christianah Adebayo-Tayo<sup>1,A,C-F</sup>, Gbemisola Elisabeth Ogunleye<sup>1,B-F</sup>, Omonike Ogbole<sup>2,C,F</sup>

<sup>1</sup> Department of Microbiology, University of Ibadan, Nigeria

<sup>2</sup> Department of Pharmacognosy, University of Ibadan, Nigeria

A – research concept and design; B – collection and/or assembly of data; C – data analysis and interpretation; D – writing the article; E – critical revision of the article; F – final approval of the article

Polymers in Medicine, ISSN 0370-0747 (print), ISSN 2451-2699 (online)

Polim Med. 2019;49(2):57–62

## Address for correspondence

Bukola Christianah Adebayo-Tayo  
E-mail: bukola.tayo@gmail.com

## Funding sources

None declared

## Conflict of interest

None declared

## Acknowledgements

We appreciate the authorities of University of Ibadan in Nigeria for providing the platform and access to some facilities used for this study.

Received on August 26, 2019

Reviewed on November 3, 2019

Accepted on January 3, 2020

## Abstract

**Background.** Green route biosynthesis of silver nanoparticles using *Trichoderma viride* (*T. viride*) filtrate (TVFSNPs) can serve as an alternative to antibiotics and as an effective drug delivery to combat cancer and act as an immune-stimulator.

**Objectives.** To biosynthesize silver nanoparticles (SNPs) with *T. viride* filtrate using green route and to characterize and determine the cytotoxic and immunomodulatory potential of nanoparticles.

**Material and methods.** *Trichoderma viride* filtrate was used for biosynthesizing SNPs. The biosynthesized SNPs were characterized using UV-visible spectroscopy, Fourier transform infrared spectroscopy (FTIR), scanning electron microscopy (SEM) and energy dispersive X-ray (EDX). The cytotoxic properties against Hep-2C and rotavirus and the immunomodulatory potential were evaluated.

**Results.** *Trichoderma viride* filtrate was able to bio-reduce AgNO<sub>3</sub> to SNPs. The surface plasmon resonance peak was at 450 nm. The presence of aldehydes, amino acids, ethers, esters, carboxylic acids, hydroxyl groups, and phenol among others indicates the capping and stabilization of proteins in the nanoparticles. The nanoparticles were spherical with a size of 0.1–10.0 nm. The EDX analysis revealed a strong signal of silver (Ag). The TVFSNPs had a cytotoxic effect on Hep2C and rotavirus in a dose-dependent manner and increased the production of immunoglobulin (Ig) A (IgA) and IgM.

**Conclusions.** *Trichoderma viride* filtrate contained some biochemicals that can bio-reduce silver nitrate (AgNO<sub>3</sub>) for SNPs biosynthesis. The anticancer and immunostimulatory potential justifies the biomedical application and biotechnological relevance of *T. viride*.

**Key words:** cytotoxicity, immunomodulation, *Trichoderma* spp, filtrate, biosynthesized silver nanoparticles

## Cite as

Adebayo-Tayo BC, Ogunleye GE, Ogbole O. Biomedical application of greenly synthesized silver nanoparticles using the filtrate of *Trichoderma viride*: Anticancer and immunomodulatory potentials. *Polim Med.* 2019;49(2):57–63. doi:10.17219/pim/116086

## DOI

10.17219/pim/116086

## Copyright

© 2020 by Wrocław Medical University

This is an article distributed under the terms of the Creative Commons Attribution 3.0 Unported (CC BY 3.0) (<https://creativecommons.org/licenses/by/3.0/>)

## Introduction

Nanobiotechnology is a new research field of biotechnology and engineering which involves which involve investigating nanoparticles synthesis which involve investigating nanoparticles synthesis and regulating the connection at a cellular level between synthetic materials and biological systems.<sup>1,2</sup> Biosynthesis of metal nanoparticles is of great interest in nanoscience.<sup>3</sup> Noble metals such as gold, silver, platinum, and lead are used in the biosynthesis of nanoparticles, in which silver (Ag) is crucial for nanoparticles biosynthesis in biomedicine.

Nanoparticles have various applications in opto-electronics, diagnostic biological probes and catalysis.<sup>3,4</sup> Nanoparticles can be synthesized chemically, physically and biologically. It is difficult to prepare silver nanoparticles (SNPs) with well-defined size using chemical methods; besides, they are toxic to the environment due to the use of toxic chemicals reducing agents such as borohydride, citrate, or other organic compounds. Physical methods give a low yield of nanoparticles, while the biological methods are eco-friendly, cost-effective have low toxicity, biocompatibility and a better control over size and shape of SNPs.<sup>5,6</sup>

Fungi like *Trichoderma viride* (*T. viride*), *Trichoderma reesei* (*T. reesei*), *Alternaria flavus* (*A. flavus*), *Aspergillus niger* (*A. niger*), *Fusarium oxysporum* (*F. oxysporum*) and *Penicillium* spp. are excellent sources of extracellular enzymes which influence nanoparticles synthesis.<sup>2,4</sup> Fungi have potential in the production of nanoparticles at a faster rate on a large scale.<sup>4</sup> *Trichoderma* spp. that frequently colonize soils, decaying wood and vegetable matter. They are the dominant part of the soil microflora in different habitats, have diverse metabolic capabilities and aggressively competitive nature.<sup>7</sup> *Trichoderma* spp. are highly resistant to biochemicals, chemicals and toxins. Most are strong opportunistic invaders, fast growing, prolific producers of spores and powerful antibiotics.<sup>8</sup> *Trichoderma* species contain strains of vast economic importance, owing to their production of antibiotics and industrial enzymes and they act as biological control agents against plant pathogens.<sup>9,10</sup> Some have an antagonistic activity against phytopathogenic fungi by using substrate colonization, antibiosis and mycoparasitism as the main mechanisms. This antagonistic potential is the basis for effective application of different *Trichoderma* strains as an alternative to chemical control against a wide variety of fungal plant pathogens.<sup>11</sup> They are prolific producers of extracellular proteins. For instance, different strains produce more than 100 different metabolites that have antibiotic activities.<sup>8</sup> Based on an eco-friendly approach, low toxicity, biocompatibility and immunomodulation, the potential of greenly synthesized nanoparticles and their applications in various fields cannot be overemphasized. However, nanoparticles can also act as an immunomodulatory agents alone or in combination with established therapeutic immunomodulatory agents. The use of fungi for the biosynthesis of SNPs

provides advantages over chemical and physical methods, as it is cost-effective and environmentally friendly, and fungi can be used on a large scale. This study involves the biosynthesis and characterization of SNPs from *T. viride* and investigates its cytotoxic properties and immunomodulatory activities.

## Material and methods

### Culture collection

*Trichoderma viride*, which were previously isolated from soil samples, were obtained from the culture collection of the Microbial Physiology and Biochemistry Laboratory, Department of Microbiology, University of Ibadan, Nigeria. The culture was kept in potato dextrose agar and the stock culture was stored at 4°C and sub-cultured from time to time.

Cancer cell lines (human rhabdomyosarcoma (RD) and laryngeal carcinoma (Hep-2C)) were supplied from the Centre for Disease Control (CDC), Atlanta, Georgia and maintained in WHO Polio Laboratory, Department of Virology, University of Ibadan, Nigeria. Ethical approval for the study was obtained from the University of Ibadan Animal Care and Use Research Ethics Committee.

### Production of cell filtrates of *Trichoderma viride*

The cell filtrate of *T. viride* was produced by inoculating pure culture of *T. viride* into a sterile malt extract broth (MEB) and incubated at 25°C for 5 days. The medium was filtered using Whatman filter paper No. 1, the crude filtrates were collected and used for further studies.

### Biosynthesis of SNPs using *Trichoderma viride*

The biosynthesis of SNPs using *T. viride* was done using modified method of Devi et al.<sup>3</sup> Fifty milliliters of the cell filtrate was mixed with 50 mL of 1 mM aqueous solution of silver nitrate (AgNO<sub>3</sub>) prepared freshly in deionized water. The whole mixture was incubated at 25°C in dark place for 2 days. A flask with no addition of Ag<sup>+</sup> was used as a control. Formation of a brown solution from a colorless solution indicates SNPs biosynthesis.

### Characterization of the biosynthesized SNPs

Formation of SNPs was observed visually for color change in comparison to control. The bio-reduction was monitored using UV-visible spectrum Lambda 25 UV/Vis spectrophotometer. UV/V with the resolution of 0.5 nm.<sup>12</sup> Fourier transform infrared spectroscopy (FTIR) was used to characterize the functional groups of SNPs. The dried



SNPs were analyzed using potassium bromide (KBr) pellet (FTIR grade) method in a ratio of 1:100. The spectrum was recorded using JASCO Corporation 2967-5 (Ishikawacho, Hachioji-shi Tokyo, Japan) FT/IR-6300 in the range of 500–4000  $\text{cm}^{-1}$  at a resolution of 4  $\text{cm}^{-1}$ .<sup>3</sup> The scanning electron microscopy (SEM) analysis of the gold-coated dried SNPs was done using a coater (JEOL, Akishima-shi, Japan; Model No. JFC-1600) and the images of SNPs were obtained using a scanning electron microscope (ZEISS EVO-MA v. 10; Carl Zeiss AG, Oberkochen, Germany).<sup>13</sup> The energy dispersive X-ray (EDX) analysis of the SNPs was done at a voltage of 4 keV and current of 350  $\mu\text{A}$ .<sup>13</sup>

## MTT assay

The cytotoxicity assay of the samples was determined using MTT (3-(4, 5-dimethyl thiazole-2yl)-2, 5-diphenyl tetrazolium bromide) assay. The cell filtrate and the SNPs biosynthesized with *T. viride* filtrate (TVFSNPs) were re-dissolved in dimethyl sulfoxide (DMSO) to give a concentration of 10 mg/mL, respectively. The stock (0.1 mL) was added to 0.9 mL of maintenance medium containing antibiotics to obtain a dilution of 1000  $\mu\text{g}/\text{mL}$  (neat). Ten-fold serial dilutions of the samples were made from the “neat” using maintenance medium as diluent to obtain different concentrations. Fifty microliters of each diluent was dispensed into 96-well microtiter plates already seeded with monolayer of RD and Hep-2C in triplicates. The plates were incubated at 37°C in a carbon-dioxide environment and the cells were observed under microscope after 72 h.

The MTT colorimetric assay was used to evaluate the reduction of viability of cell cultures in the presence and absence of metabolites. The ability of the SNPs to be cytotoxic was measured using the tetrazolium dye (MTT), which is metabolized by mitochondrial enzymes of viable (surviving) cells to an insoluble, colored formazan product. The level of metabolism that occurs in the individual well of the 96-well microtiter plate is dependent on the number of healthy viable cells present. The plates were placed on a shaker for 15 min, after which absorbance of insoluble formazan salts was assessed at 492 nm wavelength on a multi-well spectrophotometer (Titertek Uniskan, Thermo Scientific™ Multi-skan™ GO UV/Vis microplate spectrophotometer).<sup>14</sup>

## Immunomodulatory activity

This study was conducted using female Swiss albino mice aged 6 weeks, weighing 20  $\pm$  4 g. They were fed with rat pellets and given water ad libitum. The animals were allowed to acclimatize to the laboratory environment for 2 weeks and were later divided into groups for the experiment. Group 1 and 2 served as the control; Group 3 was administered with TVFSNPs and Group 4 was administered *T. viride* fungal filtrate (TVF). All the procedures used in this study conformed to the guidelines for care and use of animals in research and teaching.

## Determination of IgG, IgM and IgA

The immunoglobulin (Ig) G (IgG), IgA, IgM of the treated and untreated mice was determined by diluting the blood serum samples and the control samples in 0.9% saline (1:10). Twenty microliters of the diluted samples was added to 900  $\mu\text{L}$  of phosphate buffer and labeled sample A2. The absorbance of sample A1 was taken at 340 nm. One hundred microliters of antibody reagents was added into the prepared samples and mixed properly. The reaction mixture was incubated for 5 min. Absorbance of sample A2 and the control was taken at 340 nm.

## Statistical analysis

The analysis of variance (ANOVA) and SPSS v. 25 were used to statistically evaluate the data. Values are represented as the mean  $\pm$  standard deviation (SD) of the 3 replicates of each experiment.

## Results and discussion

### Biosynthesis and characterization of SNPs

The cell filtrate of *T. viride* was used for biosynthesis of SNPs. Figure 1 shows the visual detection of SNPs biosynthesized using filtrate from *T. viride*. Changes in color from yellow to dark brown were observed.

Nanoparticles possess more surface atoms than microparticles, which enhances their functional capabilities. Biocompatible synthesis of metal nanoparticles was encouraged to exploit the biological sources of nanoparticles, because it is cost-effective.<sup>10</sup>

The *T. viride* filtrate bio-reduced  $\text{AgNO}_3$  for SNPs biosynthesis. The bio-reduction potential of the filtrate from *T. viride* is in accordance with the work by Vahabi and Karimi,<sup>16</sup> who reported that *T. reesei* is an eco-friendly fungus which biosynthesizes SNPs in a large-scale production, in which there was a change in color from yellow to dark brown.

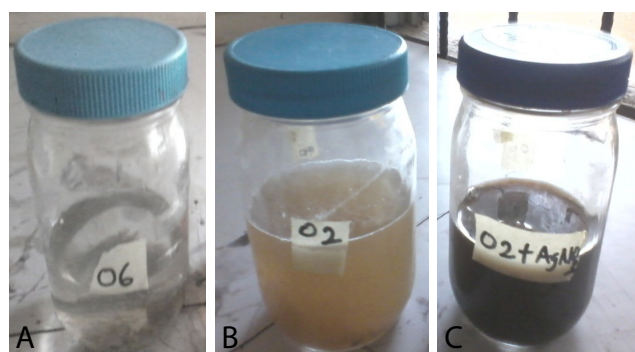


Fig. 1. Visual detection of silver nanoparticles (SNPs) biosynthesized with *Tricoderma viride* filtrate (TVFSNPs)

A – silver nitrate ( $\text{AgNO}_3$ ) solution; B – *T. viride* fungal filtrate (TVF); C – TVFSNPs.

The spectra obtained from the biosynthesized TVFSNPs are shown in Fig. 2. A broad-band spectrum between 350 nm and 550 nm was observed for TVFSNPs and the surface plasmon resonance (SPR) peak was at 450 nm, indicating the formation of SNPs.

Strong SPR is very important in the synthesis of nanoparticles and it is characterized by UV-visible absorption spectroscopy. This result is similar to the study by Kanmani and Lim,<sup>17</sup> in which SNPs showed a strong SPR peak at 400–550 nm with a broad band and size, indicating the formation of SNPs.<sup>17</sup> Guangquan et al.<sup>5</sup> reported that UV-visible spectra of the cell filtrate with AgNO<sub>3</sub> showed a strong broad peak at 440 nm, indicating the presence of SNPs.<sup>5</sup>

The FTIR analysis of TVFSNPs is shown in Fig. 3. 13 bands were present at 3425.69, 2895.25, 2359.02, 1633.76, 1404.22, 1330.93, 1149.61, 1074.39, 968.3, 931.65, 891.14, 738.76 and 597.3 cm<sup>-1</sup>. The peaks at 3245.69 cm<sup>-1</sup> and 2895.25 cm<sup>-1</sup> were attributed to O-H stretch of alcohol and C-H symmetrical stretching of aldehydes. The absorption peaks at 2359.02 cm<sup>-1</sup> and 1633.76 cm<sup>-1</sup> were also attributed to the presence of COOH overtone and the presence of C=O stretch of carboxylates. The absorption peaks at 1404.22 cm<sup>-1</sup> and 1330.93 cm<sup>-1</sup> corresponded to C-N stretch of primary amide and C-N stretch of secondary amine. The peaks at 1449.61 cm<sup>-1</sup> and 1074.39 cm<sup>-1</sup> indicated the presence of S=O sulfonic esters and C-N stretch of aliphatic amines. The absorption peaks at 968.3 cm<sup>-1</sup>, 931.65 cm<sup>-1</sup> and 891.14 cm<sup>-1</sup> corresponded to C=CH<sub>2</sub> alkenes out-of-plane bend, P-O-P stretch of pyrophosphate and C-O of epoxide. The absorption peaks at 738.76 cm<sup>-1</sup> and 597.3 cm<sup>-1</sup> indicated the presence of C-H and disulfide. From the obser-

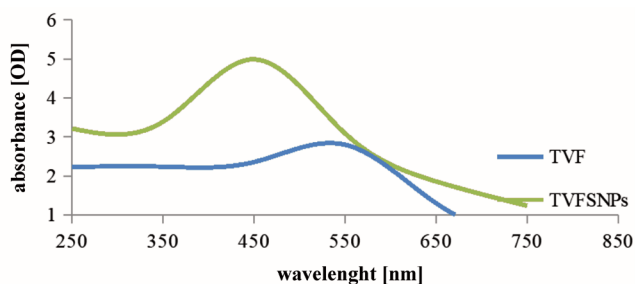


Fig. 2. UV-visible absorption spectra of TVFSNPs and TVF

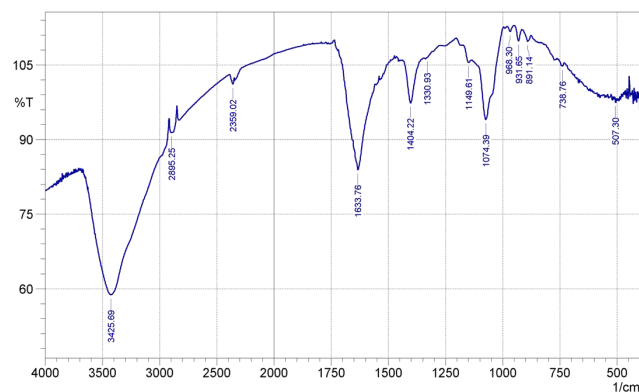


Fig. 3. Fourier transform infrared spectroscopy (FTIR) spectrum of TVFSNPs

vation in the spectrum, the presence of alcohols, aldehydes, carboxylic acids, alkenes in the samples may be responsible for the reduction of AgNO<sub>3</sub> to SNPs.

The FTIR spectra of TVFSNPs showed that different functional groups were present. Aldehydes, amino acids, ethers, esters, carboxylic acids, hydroxyl groups, phenol among others are responsible for the synthesis of SNPs. Carbonyl groups from the amino acid residues and peptides of proteins have a strong ability to bind to Ag. These proteins serve as a capping and stabilizing agent. Sonal et al.<sup>17</sup> reported that the biomolecules, especially proteins from the filtrate of *F. oxysporum*, were responsible for synthesizing and stabilizing SNPs.

The TVFSNPs were further characterized by SEM, which showed the morphology and size of the biosynthesized SNPs. The SEM micrograph is shown in Fig. 4. The TVFSNPs were spherical and 0.01–10.0 nm in size.

A scanning electron microscope is an important tool for the characterization of SNPs.<sup>15–18</sup> The shape of the TVFSNPs is in agreement with the study by Amal and Azzah,<sup>2</sup> who reported that nanoparticles are spherical with a small percentage of elongated particles with a variation in particle size, 5 nm for *F. oxysporum*, 20 nm for *A. niger* and 25 nm *Alternaria solani* (*A. solani*).

The EDX analysis of biosynthesized TVFSNPs is shown in Fig. 5. Silver had the highest intensity in the range 0.0001–0.2574.

The EDX analysis was used to determine the elemental composition of samples. Strong signals from Ag atoms in the nanoparticles were observed, while there were weaker signals from carbon, oxygen, sulfur, phosphorus, magnesium and sodium atoms. The presence of a strong Ag peak is a result of SPR. The carbon, oxygen, sulfur, phosphorus, magnesium and sodium signals may be due to the X-ray emission from proteins or enzymes present in the cell wall of the organisms. The presence of other EDX peaks for chlorine, sodium and oxygen was as a result of mixed precipitates present in the extract. Pnyabrata et al. had similar report.<sup>19–20</sup>

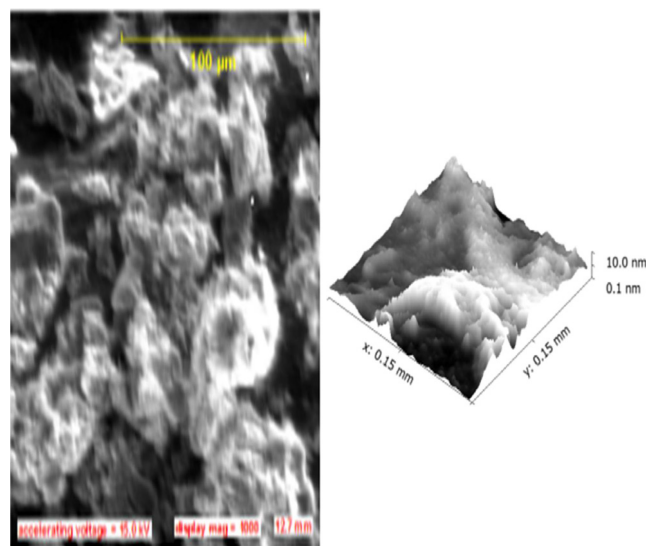


Fig. 4. A scanning electron micrograph of TVFSNPs

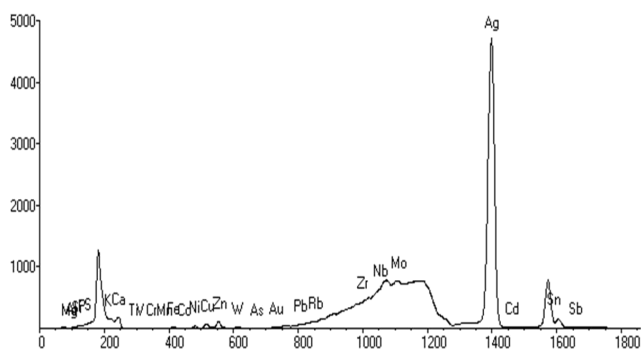


Fig. 5. Energy dispersive X-ray (EDX) analysis of TVFSNPs

## Cytotoxicity assay of the TVFSNPs against Hep-2C and rotavirus cell lines

Cytotoxicity activity against hepatitis-2C (Hep-2C) and rotavirus cell lines was evaluated at different concentrations by MTT assay. Table 1 shows the  $IC_{50}$  ( $\mu\text{g/mL}$ ) and dose-dependent values for the in vitro cytotoxic activity against Hep-2C cell lines. It was observed that TVFSNPs inhibited the viability of Hep-2C cell lines in dose-dependent manner. Silver nanoparticles were not toxic at lower doses, while mild cytotoxicity was recorded at higher doses.

Table 2 shows the  $IC_{50}$  ( $\mu\text{g/mL}$ ) and dose-dependent values for the in vitro cytotoxic activity against rotavirus cell lines. The TVFSNPs did not exhibit significant cytotoxicity at their lower concentrations, while cytotoxicity increased at higher concentrations.

Cytotoxicity increased at higher TVFSNPs concentrations. The ability of the TVFSNPs to increase toxicity at a higher concentration may be due to metal nanoparticles overaccumulating inside the cell. It may also be due to the fact that SNPs interfere with the proper functioning of cellular proteins and induce subsequent changes in cellular chemistry. The cytotoxicity impact of SNPs in biological systems depends on their physiochemical properties.<sup>21</sup>

Vimbela et al.<sup>22</sup> reported a dose-dependent cytotoxicity effect of nanoparticles against J774 and THPI cell lines, in which there were no cytotoxic effects at low doses (10  $\mu\text{g}$ ), whereas mild cytotoxicity effects were observed at high doses of 100–150  $\mu\text{g}$ . Raman et al. reported the dose-dependent cytotoxicity potential of *Melia azedarach* SNPs against HeLa cells.<sup>24</sup>

The anti-proliferative effect of SNPs on cancer cell line has been reported.<sup>24,25</sup> Choi et al. reported the cytotoxicity potential of SNPs on A2780 ovarian carcinoma cells and ovarian cancer stem cells at a high concentration. The cells are more sensitive to the treatment with SNPs.<sup>25</sup>

## Immunomodulatory activity of TVSNPs

The immunomodulatory activity of the fungal filtrate and TVFSNPs is shown in Table 3. There was a significant difference in the immunomodulatory activity of the treatments using the biosynthesized TVFSNPs and the TVF on the treated mice.

Group 2, which included mice treated with sheep red blood cells, had the highest IgG. The IgA of the treated mice ranged from 75 to 258 mg/dL. Group 3 (mice treated with TVFSNPs) had the highest IgG, while Group 4 (mice treated with TVF) had the lowest IgG. The IgM of the treated mice ranged from 96 to 24 mg/dL. Group 3 had the highest IgM, while Group 4 had the lowest IgM.

The immunomodulatory potential of TVFSNPs based on in vivo immunological activity was investigated. The TVFSNPs showed significant immunostimulation of IgA and IgM. The ability of TVFSNPs to stimulate IgA and IgM in the immune system of the mice may be due to the easy engulfment of macrophages to the SNPs. Serum glycoproteins are stimulated to produce a subpopulation of white blood cells called lymphocytes. This could be as a result of the nanoparticles stimulating macrophages activity which evolve from immune system to protect

Table 1.  $IC_{50}$  ( $\mu\text{g/mL}$ ) and dose-dependent values for the in vitro cytotoxic activity against Hep-2C cell lines

Samples	Concentration [ $\mu\text{g/mL}$ ] $\pm$ SEM						$IC_{50}$ [ $\mu\text{g/mL}$ ]
	0.01	0.1	1	10	100	1000	
AgNO <sub>3</sub>	0.627 $\pm$ 0.02 <sup>c</sup>	25.013 $\pm$ 0.21 <sup>a</sup>	27.729 $\pm$ 0.03 <sup>b</sup>	34.036 $\pm$ 0.02 <sup>b</sup>	38.46 $\pm$ 0.04 <sup>d</sup>	55.793 $\pm$ 0.03 <sup>c</sup>	50.02 $\pm$ 0.02 <sup>b</sup>
TVFSNP	0.623 $\pm$ 0.01 <sup>c</sup>	8.591 $\pm$ 0.02 <sup>c</sup>	20.348 $\pm$ 0.06 <sup>d</sup>	26.823 $\pm$ 0.04 <sup>d</sup>	47.89 $\pm$ 0.21 <sup>c</sup>	51.146 $\pm$ 0.03 <sup>d</sup>	54.27 $\pm$ 0.02 <sup>a</sup>
TVF	1.316 $\pm$ 0.03 <sup>b</sup>	5.406 $\pm$ 0.01 <sup>d</sup>	22.187 $\pm$ 0.06 <sup>c</sup>	27.583 $\pm$ 0.02 <sup>c</sup>	49.756 $\pm$ 0.09 <sup>b</sup>	69.303 $\pm$ 0.04 <sup>a</sup>	37.83 $\pm$ 0.03 <sup>d</sup>
CTX	20.163 $\pm$ 0.05 <sup>a</sup>	22.75 $\pm$ 0.03 <sup>b</sup>	41.093 $\pm$ 0.08 <sup>a</sup>	54.556 $\pm$ 0.09 <sup>a</sup>	73.546 $\pm$ 0.24 <sup>a</sup>	67.946 $\pm$ 0.02 <sup>b</sup>	47.19 $\pm$ 0.02 <sup>c</sup>

SEM – scanning electron microscopy; CTX – anticancer drug. Data presented as mean  $\pm$  standard deviation (SD).

Table 2.  $IC_{50}$  ( $\mu\text{g/mL}$ ) and dose-dependent values for the in vitro cytotoxic activity of against rotavirus cell lines

Samples	Concentration [ $\mu\text{g/mL}$ ] $\pm$ SEM						$IC_{50}$ [ $\mu\text{g/mL}$ ]
	0.01	0.1	1	10	100	1000	
AgNO <sub>3</sub>	2.083 $\pm$ 0.02 <sup>c</sup>	17.951 $\pm$ 0.02 <sup>b</sup>	22.386 $\pm$ 0.02 <sup>c</sup>	24.113 $\pm$ 0.02 <sup>c</sup>	25.163 $\pm$ 0.03 <sup>c</sup>	96.606 $\pm$ 0.02 <sup>a</sup>	31.00 $\pm$ 0.06 <sup>c</sup>
TVFSNP	2.976 $\pm$ 0.02 <sup>b</sup>	19.956 $\pm$ 0.02 <sup>a</sup>	27.786 $\pm$ 0.03 <sup>b</sup>	32.016 $\pm$ 0.03 <sup>b</sup>	35.206 $\pm$ 0.03 <sup>b</sup>	82.256 $\pm$ 0.03 <sup>d</sup>	38.33 $\pm$ 0.04 <sup>b</sup>
TVF	3.883 $\pm$ 0.03 <sup>a</sup>	12.689 $\pm$ 0.03 <sup>c</sup>	18.156 $\pm$ 0.04 <sup>d</sup>	20.653 $\pm$ 0.03 <sup>d</sup>	22.662 $\pm$ 0.02 <sup>d</sup>	86.146 $\pm$ 0.02 <sup>b</sup>	28.54 $\pm$ 0.03 <sup>d</sup>
CTX	3.612 $\pm$ 0.02 <sup>a</sup>	9.475 $\pm$ 0.03 <sup>d</sup>	34.533 $\pm$ 0.02 <sup>a</sup>	55.303 $\pm$ 0.02 <sup>a</sup>	73.173 $\pm$ 0.02 <sup>a</sup>	84.596 $\pm$ 0.03 <sup>c</sup>	49.05 $\pm$ 0.02 <sup>a</sup>

**Table 3.** Immunomodulatory activity of TVFSNPs

S/N	Group	SRBC	SNPs	FF	IgG [mg/dL]	IgA [mg/dL]	IgM [mg/dL]
1	GRP1a	-	-	-	0.000	0.000	0.000
2	GRP1b	-	-	-	79 ±0.65 <sup>b</sup>	171 ±0.97 <sup>c</sup>	38 ±0.12 <sup>c</sup>
3	GRP2	+	-	-	118 ±0.23 <sup>a</sup>	230 ±0.45 <sup>b</sup>	73 ±0.26 <sup>b</sup>
4	GRP3	-	+	-	48 ±0.27 <sup>d</sup>	258 ±0.73 <sup>a</sup>	96 ±0.22 <sup>a</sup>
5	GRP4	-	-	+	63 ±0.39 <sup>c</sup>	75 ±0.81 <sup>d</sup>	24 ±0.17 <sup>d</sup>

n = 6; p < 0.05 – significant difference; GRP1a – mice not exposed to cigarette smoke and not treated; GRP1b – mice exposed to cigarette smoke and not treated; GRP2 – mice administered sheep red blood cells; GRP3 – mice administered TVFSNPs; GRP4 – mice administered TVF; SNPs – silver nanoparticles; FF – fungal filtrate; SN – serial number, SRBC – sheep red blood cell.

the host from potentially pathogenic agents, eliminate neoplastic cells and to reject non-self-components. Swarnakar et al. reported that the chemically synthesized nanoparticles act as an immunomodulatory agent alone or in combination with established therapeutic immunomodulatory agents, and can be a targeted drug/vaccine delivery vehicle to macrophages.<sup>27</sup>

## Conclusions

The filtrate from *T. viride* mediated the biosynthesis of SNPs, which were spherical in shape and nontoxic at a lower concentration. The TVSNPs exhibited cytotoxicity against Hep-2C cell line and RD cell line in a dose-dependent manner and had immune-stimulation potential by increasing the production of IgA and IgM. The anticancer and immunomodulatory potential of TVSNPs justifies its biomedical application and showcases the biotechnological relevance of the fungus.

## ORCID iDs

Bukola Christianah Adebayo-Tayo

<https://orcid.org/0000-0003-2404-1686>

Gbemisola Elizabeth Ogunleye <https://orcid.org/0000-0003-2344-8177>

Omonike Ogbole <https://orcid.org/0000-0002-6487-9494>

## References

- Juhi S, Madan MS, Sarika G, Abhijeet S. Emerging role of fungi in nanoparticles synthesis and their applications. *World J Pharm Sci.* 2014;(3)9:1586–1613.
- Amal AAJ, Azzah AG. Biosynthesis of silver nanoparticles by *Aspergillus niger*, *Fusarium oxysporum* and *Alternaria solani*. *Afri J Biotechnol.* 2015;(4):2170–2174.
- Devi TP, Kulanthaivel S, Kamil D, Borah JL, Prabhakaran N. Biosynthesis of silver nanoparticles from *Trichoderma* species. *India J Experimental Biol.* 2013;(51)7:543–547.
- Nikalje AP. Nanotechnology and its application in medicine. *Medicinal Chem.* 2015;5:81–89.
- Guangquan L, Dan H, Yongang Q, et al. Fungus-mediated green synthesis of silver nanoparticles using *Aspergillus terreus*. *Intern J Molecular Sci.* 2012;(13):466–467.
- Sandhu SS, Shukla H, Shukla S. Biosynthesis of silver nanoparticles by endophytic fungi: Its mechanism, characterization techniques and antimicrobial potential. *African J Biotechnol.* 2017;(16)14:683–698.
- Samuels GJ. *Trichoderma*: Systematics, the sexual state and ecology. *Phytopathology.* 2006;(96)2:195–206.
- Harman GE, Howel CR, Viterbo A, Chet I, Lorito M. *Trichoderma* species – opportunistic, virulent plant symbionts. *Nature Review Microbiol.* 2004;(2):43–55.
- Druzhinina IS, Komon-Zelazowska M, Ismaiel A, et al. Molecular phylogeny and species delimitation in the section *Longibrachiatum* of *Trichoderma*. *Fungal Genetic Biol.* 2012;(49)5:358–368.
- Sivasithamparam K, Ghisalberti E. Secondary metabolism in *Trichoderma* and *Gliocladium*. In: Kubicek CP & Harman GE (eds.), *Trichoderma and Gliocladium*. 1998;1:139–191. London, UK: Taylor & Francis.
- Babu K, Pallavi PN. Isolation, identification and mass multiplication of *Trichoderma* – an important bio-control agent. *Inter J Pharmacy Life Sci.* 2013;(4)1:2320–2323.
- Ottoni CA, Simões MF, Fernandes S, et al. Screening of filamentous fungi for antimicrobial silver nanoparticles synthesis. *AMB Express* 2017;7:31–41.
- Natarajan K, Selvaraj S, Murty VR. Microbial production of silver nanoparticles. *DIG J Nanomater Bios.* 2010;(5)1:135–140.
- Nikhil SS, Mahesh B, Rahul B, et al. Biosynthesis of silver nanoparticles using extract from the producing fungal strain. *Process Biochem.* 2009;45:939–943.
- Sukirtha R, Priyanka KM, Antony JJ, et al. Cytotoxic effect of green synthesized silver nanoparticles using *Melia azedarach* in vitro HeLa cell lines and lymphoma mice model. *Process Biochem.* 2010;11:1–34.
- Vahabi Ali MG, Karimi, S. Biosynthesis of silver nanoparticles by fungus *Trichoderma reesei* used for large scale production of Ag nanoparticles. *Intern J Nanosci.* 2011;(1)1:65–79.
- Kanmani P, Lim ST. Synthesis and structural characterization of silver nanoparticles using bacterial activity against food and multidrug resistant pathogens. *Process Biochem.* 2013;(48):1099–1106.
- Sonal SB, Swapnil C, Aniket KG, Mahendra KR. Rapid synthesis of silver nanoparticles from *Fusarium oxysporum* by optimizing physico-cultural conditions. *ScientificWorldJournal.* 2013;(10):1155–1167.
- Nanda A, Raghavan CM. Antimicrobial efficacy of synthesized AgNPs from exopolysaccharides (EPS) produced by *Bacillus subtilis* of medico-clinical sinks. *Intern J Chemical Technol Res.* 2014;(6)5:2914–2919.
- Pnyabrata M, Absar A, Deendayal M, et al. Fungus-mediated synthesis of silver nanoparticles and their immobilization in the mycelia matrix: A novel biological approach to nanoparticle synthesis. *Nano Lett.* 2001;(1)10:515–519.
- Usha MC, Gladys ARD. Biogenic synthesis of silver nanoparticles by *Acacia nilotica* and their antibacterial activity. *Intern J Scientific Res.* 2014;(3)6:27–29.
- Vimbela GV, Ngo SM, Frazee C, Yang L, Stout DA. Antibacterial properties and toxicity from metallic nanomaterials. *Inter J Nanomed.* 2017;(12):3941–3965.
- Faria F, Preeti B, Neelam P, Sarika S, Shivam P, Smita RV. Antimicrobial and immunomodulatory efficacy of extracellularly synthesized silver and gold nanoparticles by a novel phosphate solubilizing fungus *Bipolaris tetramera*. *BMC Microbiology.* 2015;(15):52.
- Raman S, Muthukalingn K, Rajamanickam R, Sound AK, Palanivel K. Derived silver nanoparticles: A novel antitumor agent against Dalton's ascites lymphoma. *Intern J Green Nanotechnol.* 2012;(1)3:2–12.
- Choi YJ, Lee HW, Lee YS, Shim da M, Seo SW. Differential cytotoxic potential of silver nanoparticles in human ovarian cancer cells and ovarian cancer stem cells. *Int J Mol Sci.* 2016;(17)12:2077.
- Kovacs D, Szoke K, Igaz N, et al. Silver nanoparticles modulate ABC transporter activity and enhance chemotherapy in multidrug resistant cancer. *Nanomedicine.* 2016;12(3):601–610.
- Swarnakar N, Thanki K, Jain S. Effect of co-administration of CoQ10-loaded nanoparticles on the efficacy and cardio-toxicity of doxorubicin-loaded nanoparticles. *RSC Adv.* 2013;3:146–171.

# Strategy to modulate the tumor microenvironment using nanoparticles

Harshita Agrawal<sup>A–F</sup>, Rishabha Malviya<sup>A–F</sup>, Pramod Kumar Sharma<sup>A–F</sup>

Galgotias University, Greater Noida, India

A – research concept and design; B – collection and/or assembly of data; C – data analysis and interpretation; D – writing the article; E – critical revision of the article; F – final approval of the article

Polymers in Medicine, ISSN 0370-0747 (print), ISSN 2451-2699 (online)

*Polim Med.* 2019;49(2):63–66

## Address for correspondence

Harshita Agrawal

E-mail: harshita28497@gmail.com

## Funding sources

None declared

## Conflict of interest

None declared

## Acknowledgements

Authors are highly thankful to the Department of Pharmacy, School of Medical and Allied Sciences, Galgotias University Greater Noida for providing library facilities.

Received on March 23, 2019

Reviewed on May 6, 2019

Accepted on September 15, 2019

## Abstract

Tumors are considered as one of the deadliest diseases to affect the human body. Nowadays, nanoparticles, which are based on enhanced permeability and retention, have become prevalent in the treatment of tumors, as they have numerous advantages over conventional treatments of tumors. Recently, it has been reported that tumors are complex networks which comprise of neoplastic as well as non-neoplastic cells. The non-neoplastic cells, collectively called as stroma, assists in tumor progression and also in their survival. In this review, we summarize the strategies which help to modulate the tumor microenvironment in order to enhance nanoparticle delivery for the treatment of a tumor; this comprises of three main factors: improving tumor perfusion, facilitating nanoparticles extravasation and enhancing interstitial transport of nanoparticles. These strategies are beneficial due to the development of a new combination of therapeutic agents. The major role of the tumor microenvironment at the time of initiation and progression is to modify the fundamentals of tumor biology and also to improve molecular diagnostics and therapeutics. This review emphasizes the properties and characteristics of the tumor microenvironment that are utilized to develop drug delivery systems by nanotechnology, which aim to target tumor cells and tumor microenvironment.

**Key words:** nanoparticles, tumor stroma, tumor perfusion, tumor vessel normalization, tumor vessel disruption

## Cite as

Agrawal H, Malviya R, Sharma PK. Strategy to modulate the tumor microenvironment using nanoparticles.

*Polim Med.* 2019;49(2):63–66. doi:10.17219/pim/112356

## DOI

10.17219/pim/112356

## Copyright

© 2020 by Wrocław Medical University

This is an article distributed under the terms of the Creative Commons Attribution 3.0 Unported (CC BY 3.0)

(<https://creativecommons.org/licenses/by/3.0/>)

## Introduction

A tumor is defined as a self-determining, sovereign disease of neoplastic cells. In recent days, the delivery of nanoparticle to cancerous cells has attracted vast attention in the field of the treatment of tumor.<sup>1</sup> Nanoparticles show advantages over drugs which is based on enhanced permeability and retention (EPR) effect. The basic properties of EPR are highly permeable tumor vessels that allows the permeability of particles which includes proteins, micelles, macromolecules, liposomes and other particles that are large enough to avoid renal clearance and causes enhanced retention of those extravagated particles.<sup>2</sup> Therefore, the main principle behind targeting with EPR effect that tumor targeted by nanoparticles delivery has gained huge success. Extensive literature discloses that EPR drug delivery was compromised by tumor microenvironment (TME).<sup>3</sup> Tumor microenvironment is characterized by irregular vascular distribution, poor blood flow, elevated tumor interstitial fluid pressure, rich matrix, and abundant tumor stroma cells. The tumor microenvironment is an important part of tumor tissues, which functions as the soil for the seeds; it is the tumor microenvironment that is responsible for tumor cells proliferating, differentiating and promoting tumor growth. The TME consists of varieties of cells, namely, fibroblasts, myofibroblasts, adipocytes, immune cells, blood vasculature, lymphatic vasculature, and extracellular matrix.<sup>4</sup> The tumor microenvironment and its cells have some significant irregularities, such as an acidic pH, hyperthermia, altered redox potential, up-regulated proteins, which can have an antitumor application, that is, by using stimulus-responsive nanopreparations.<sup>5</sup> Thus, nanotechnology has become a developing field for stimulus-responsive nanopreparations in tumors, employing the altered tumor microenvironment to ease the accumulation of provided chemotherapy at the tumor site, which allows for the specific targeting of the tumor and also enables tumor microenvironment to achieve tumor growth inhibition.<sup>6</sup> It is important to understand the basic difference between a tumor and cancer. In cancer the cellular growth is uncontrollable and it also spreads all over the body, but in the case of tumor, cancer develops when lump is formed inside the body due to abnormal cellular growth. A tumor may or may not develop into cancer. A tumor converts into cancer when it is malignant.

This literature will focus on the strategies applied to modulate the immune response as well as various aspects of TME targeted by nanoparticles. Extensive literature survey reflects that the tumor microenvironment plays a crucial role in the development, proliferation, and metastasis of tumors. Many of the conventional therapies designed to eradicate tumors fail because of the tumor microenvironment; therefore, nanoparticles take a lead into the properties of the tumor microenvironment.<sup>7</sup> Different strategies are applied to improve the therapeutic benefits

of nanoparticles, which include employing active targeting nanoparticles, developing tumor-responsive drugs, optimizing the physiochemical parameters of nanoparticles, such as their shape, charge, and size. This review focuses on immune response modulating and also TME aspects targeted by nanoparticles delivery. The TME is framed by developing a tumor, and for tumor progression, both the cells, i.e., tumor cells as well as stroma cells, are provide benefit. Therefore, the logic for developing stroma cells at the tumor site has not been understood clearly. Stroma cells are basically a collection of cells which consist of immune cells, smooth muscle, vascular muscle, fibroblasts, endothelial, as well as extracellular matrix, along with the secreted molecules which behave in paracrine and autocrine manners to enhance the survival of tumor cells.<sup>8</sup> The growth of the tumor is revitalized by some of the growth factors and also by chemokines, which are produced by the immune cells in the stroma and also altered fibroblasts, which then engage more stromal cells. Consequently, the TME modification was considered as an important tool for nanomedicine delivery improvement. Hence, it is reported that delivery of the nanoparticles to the site of the tumor is based on two types of mechanism, namely active and passive mechanism. In a passive mechanism, nanoparticles, which have properties of long systemic circulation, have the ability to assemble in the interstitial space, where the selective collection is attained by enhanced permeability and retention effect. In the case of active mechanism, the nanoparticles are attached with molecular ligands, such as cell specific ligands, biological proteins, antibodies, peptides, etc. These ligands improve the cellular uptake of nanoparticles via receptor-mediated endocytosis.<sup>9-11</sup>

## Strategies to modulate tumor microenvironment

There are several strategies used for modulating tumor microenvironment to enhance the nanoparticles delivery for the treatment of tumor and they are divided into the following three categories: improving tumor perfusion, facilitating nanoparticles extravasation and enhancing interstitial transport of nanoparticles (Fig. 1).<sup>1</sup>

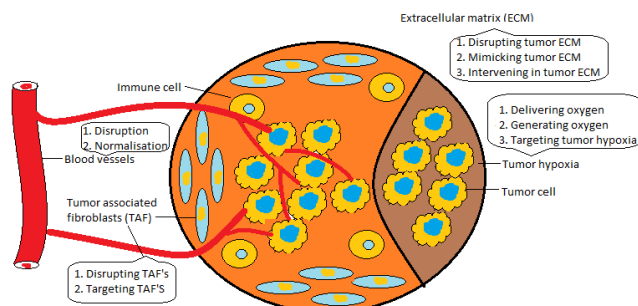


Fig. 1.

## Tumor vessel normalization

The newly formed tumor vessels are always curvy and drippy, which allows nanoparticles extravasation, but, at the same time, this increases interstitial fluid pressure, which helps in preventing adequate blood flow of nanoparticles. The goal is to improve nanoparticle delivery for the treatment of a tumor; for this the vessels need to be normalized, which has been found to be an efficacious approach to improve nanoparticle delivery. During normalization of vessels, the abnormal phenotype of tumor vessels transforms into the phenotype, which seems to closely resemble functional normal vessels by mending the basement membrane and increasing coverage rate of pericytes and eventually decreases leakiness of vessel.<sup>12</sup> Hence, optimization in the tumor vessel structure can ultimately decrease the extravasation of fluid and also lowers interstitial fluid pressure and this cause's tumor blood flow to restore which can improve vascular transport of nanoparticles (Fig. 1). In this review, 4 strategies have been discussed for vessel normalization to improve nanoparticle delivery for the treatment of the tumor. The foremost strategy is capable of improving only the delivery of drugs which have a small molecular weight or drugs which have a small molecular weight compared to the nanoparticles, which range from 20 to 40 nm, but minimizes the delivery of nanoparticles which have a large molecular weight.<sup>13</sup> This occurs because large nanoparticles reduce the endothelial gap of vessels of the tumor. The treatment for a tumor in the second strategy by nanoparticles is delivered during the normalization window. The treatment for a tumor in the second strategy by nanoparticles is delivered during the normalization window. Thirdly, it is necessary to prevent excessive elimination of tumor vessels; in order to achieve this appropriate dose of vascular normalizer is highly recommended. Lastly, this strategy is only applicable in the case of highly permeable tumors and not for desmoplastic tumors, because, as we know, vasculatures are highly constricted in the desmoplastic tumors.<sup>14</sup>

## Tumor vessel disruption

In tumor tissues, vasoconstriction arbitrates via vasoconstrictive endothelin-1 (ET1) and also via its receptor, i.e., ETA, which is essential for maintaining the contractile tone of tumor vessels. The articulation level of ETA and ET1 for tumor vessels was found to be 13-fold and 5-fold elevated than normal vessels size.<sup>15</sup> Therefore, a selective antagonist, i.e., BQ123, inhibits signaling between ET1 and ETA and tumor vessel dilation, and it also triggers a tumor-specific increase in blood flow. The increase in blood flow is caused by BQ123, which can improve the delivery of the free drug to tumors. Moreover, it was found that BQ123 can increase nanoparticle delivery for tumor treatment.<sup>16</sup>

## Inflammatory mediators

Tumor necrosis factor alpha, VEGF, and nitric oxide (NO) donors<sup>17</sup> are some of the inflammatory mediators which have the ability to enhance vascular permeability. This enhanced vascular permeability can be used to enhance the accumulation of nanoparticles in tumors higher than control group, i.e., 2 to 6-fold higher. After vascular permeability is enhanced, vasodilatation and blood flow need to improve. This improvement occurs by means of inflammatory mediators. These inflammatory mediators, which give a series of effect, can also participate in the elevation of interstitial fluid pressure against nanoparticles delivery.<sup>17</sup> Hence, the accumulation of nanoparticles in tumor cells apparently depends on these factors.

## Depletion of pericyte

In a desmoplastic tumor, pericytes coverage rates on endothelium were about 70% higher than in highly permeable tumors, which ultimately restricts the transvascular movement of nanoparticles into tumor interstitium. Therefore, certain strategies are being developed to reduce the coverage rate of pericytes of the endothelium by using a low dose of an LY36947 and TGF- $\beta$  and also to increase size gaps between the endothelium. This can increase the therapeutic benefits of many drugs.<sup>18</sup> In a literature review, therapeutic benefits of gemcitabine loaded liposomes delivered for pancreatic tumor and also Doxil-loaded liposomes for diffusion type gastric tumor have been reported.<sup>1</sup>

## Depletion of platelets

It is known that homeostasis is triggered by platelets, which play the primary role in thrombus formation. Apart from this role, platelets also contribute to tumor progression and metastasis. Additionally, tumor vascular homeostasis is also supported by platelets as well as the integrity of tumor vessels.<sup>19</sup> Extensive studies have revealed that a reduced number of platelets causes severe blood flow at the tumor site and can also causes leakiness of tumor vasculature. A study has reported that, platelets reduction in thrombocytopenic mice increase efficiency of chemotherapy for breast cancer. Another study has found that TME responsive nanoparticles have the ability to deliver antibodies to deplete the selective platelet in tumor tissues; this was done to avoid bleeding in normal organs of the body.<sup>20</sup> Following this, vascular permeability was augmented and, as a result, nanoparticle delivery for tumor treatment was improved. It has been concluded that the depletion of platelets is a reliable means of augmenting transvascular delivery for treatment of tumors through nanoparticles.<sup>21</sup>

## Physical stimulus

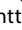
Physical stimulus includes radiation, which can improve nanoparticles delivery for tumor.<sup>22</sup> A literature survey reveals that there are various mechanisms wherein radiation can regulate the growth of vascular endothelial factor, and this is regulated by activating the HIF1 factor, i.e., the hypoxia-inducible factor 1, and also by multiple mitogen-activated protein kinase-dependent pathways which enhance tumor vessel permeability.<sup>23</sup> Therefore, after an extensive literature survey, results have revealed that permeability of tumor vessels permeability of imaging-contrast agent with the molecular weight above 200 kDa was increased by 32.8% after irradiation. Moreover, radiation has the capacity to kill the tumor cells, which are sensitive in nature. It is concluded that the density of cells helped in diminishing compression stress of tumor cells and hence enhancing the blood flow of tumors, and the effect of radiation on tumors is dependent on the dose, time and tumor type.<sup>24,25</sup>


## Conclusions

Nanoparticle drug delivery has attracted considerable attention in the treatment of tumors. Nanoparticles in the tumor microenvironment provide a universal approach for anti-tumor therapy. Tumors are highly heterogeneous and, hence, growth is done in a complex microenvironment. The responsive peptide-base nanoformulations are also used for Improved Tumor Therapy. Tumor microenvironment consists of fibroblasts, immune cells, and extracellular matrix components. It is pivotal to formulate nanoparticles for a tumor which can easily adapt the tumor microenvironment and enhance the targeting of the drugs to the tumor cells. Recent advancements have been made in nanoparticle technology, allowing the development of tumor vasculature-targeted drug delivery, which can enhance the therapeutic efficacy of various anti-tumor medicines. Nanoparticles can directly affect the immune cells as well also their responses within the TME and they can also be functionalized to improve the particular subpopulations of immune cells, such as NK cells, DCs, and T cells.

### ORCID iDs

Harshita Agrawal  <https://orcid.org/0000-0001-5340-6328>

Rishabha Malviya  <https://orcid.org/0000-0003-2874-6149>

Pramod Kumar Sharma  <https://orcid.org/0000-0002-2418-7055>

### References

- Zhang B, Hu Y, Pang Z. Modulating the tumor microenvironment to enhance tumor nanomedicine delivery. *Front Pharmacol*. 2017;8:1–16.
- Allen TM, Cullis PR. Drug delivery systems: Entering the mainstream. *Science*. 2004;303(5665):1818–1822.
- Barenholz YC. Doxil<sup>®</sup>—the first FDA-approved nano-drug: Lessons learned. *J Control Release*. 2012;160(2):117–134.
- Albini A, Sporn MB. The tumor microenvironment as a target for chemoprevention. *Nat Rev Clin*. 2007;7(2):139.
- Zhu L, Torchilin VP. Stimulus-responsive nanopreparations for tumor targeting. *Integr Biol*. 2013;5(1):96–107.
- Cho K, Wang XU, Nie S, Shin DM. Therapeutic nanoparticles for drug delivery in tumor. *Clin Tumor Res*. 2008;14(5):1310–1316.
- Siegler EL, Kim YJ, Wang P. Nanomedicine targeting the tumor microenvironment: Therapeutic strategies to inhibit angiogenesis, remodel matrix, and modulate immune responses. *J Cell Immunother*. 2016;2(2):69–78.
- Roy A, Li SD. Modifying the tumor microenvironment using nanoparticle therapeutics. *Nanomed Nanobiotechnol*. 2016;8(6):891–908.
- McMillin DW, Delmore J, Weisberg E, et al. Tumor cell-specific bioluminescence platform to identify stroma-induced changes to antitumor drug activity. *Nat Med*. 2010;16(4):483.
- Teicher BA, Herman TS, Holden SA, et al. Tumor resistance to alkylating agents conferred by mechanisms operative only in vivo. *Science*. 1990;247(4949):1457–1461.
- Fidler IJ, Wilmanns C, Staroselsky A, Radinsky R, Dong Z, Fan D. Modulation of tumor cell response to chemotherapy by the organ environment. *Tumor Metast Rev*. 1994;13(2):209–222.
- Goel S, Duda DG, Xu L, Munn LL, Boucher Y, Fukumura D, Jain RK. Normalization of the vasculature for treatment of tumor and other diseases. *Physiol Rev*. 2011;91(3):1071–1121.
- Chauhan VP, Stylianopoulos T, Martin JD, et al. Normalization of tumor blood vessels improves the delivery of nanomedicines in a size-dependent manner. *Nat Nanotech*. 2012;7(6):383–388.
- Zhang B, Shi W, Jiang T, et al. Optimization of the tumor microenvironment and nanomedicine properties simultaneously to improve tumor therapy. *Oncotarget*. 2016;7(38):62607.
- Sonveaux P, Dessy C, Martinive P, et al. Endothelin-1 is a critical mediator of myogenic tone in tumor arterioles: Implications for tumor treatment. *Tumor Res*. 2004;64(9):3209–3214.
- Martinive P, De Wever J, Bouzin C, et al. Reversal of temporal and spatial heterogeneities in tumor perfusion identifies the tumor vascular tone as a tunable variable to improve drug delivery. *Mol Tumor Ther*. 2006;5(6):1620–1627.
- Seki T, Fang J, Maeda H. Enhanced delivery of macromolecular antitumor drugs to tumors by nitroglycerin application. *Tumor Sci*. 2009;100(12):2426–2430.
- Kano MR, Bae Y, Iwata C, Morishita Y, Yashiro M, Oka M. Improvement of cancer-targeting therapy, using nanocarriers for intractable solid tumors by inhibition of TGF-beta signaling. *Proc Natl Acad Sci U.S.A.* 2007;104:3460–3465.
- Huang Y, Yuan J, Righi E, et al. Vascular normalizing doses of anti-angiogenic treatment reprogram the immunosuppressive tumor microenvironment and enhance immunotherapy. *Proc Natl Acad Sci*. 2012;109(43):17561–17566.
- von Maltzahn G, Park JH, Lin KY, et al. Nanoparticles that communicate in vivo to amplify tumour targeting. *Nat Mater*. 2011;10:545–552.
- Demers M, Ho-Tin-Noé B, Schatzberg D, Yang JJ, Wagner DD. Increased efficacy of breast tumor chemotherapy in thrombocytopenic mice. *Tumor Res*. 2011;71(5):1540–1549.
- Eikenes L, Tari M, Tufto I, Bruland OS, de Lange Davies C. Hyaluronidase induces a transcapillary pressure gradient and improves the distribution and uptake of liposomal doxorubicin (Caelyx<sup>™</sup>) in human osteosarcoma xenografts. *Br J Tumor*. 2005;93(1):81.
- Moeller BJ, Cao Y, Li CY, Dewhirst MW. Radiation activates HIF-1 to regulate vascular radiosensitivity in tumors: role of reoxygenation, free radicals, and stress granules. *Tumor Cell*. 2004;5(5):429–441.
- Stapleton S, Jaffray D, Milosevic M. Radiation effects on the tumor microenvironment: implications for nanomedicine delivery. *Adv Drug Deliv Rev*. 2016;109:119–130.
- Qin H, Ding Y, Mujeeb A, Zhao Y, Nie G. Tumor microenvironment targeting and responsive peptide-based nanoformulations for improved tumor therapy. *Molecular Pharmacology*. 2017;92(3):219–231.



# The use of different dialysis membranes in therapy of patients with multiple myeloma

Maciej Szymczak<sup>1,A–F</sup>, Dorota Zielińska<sup>2,D,F</sup>, Aleksandra Musiała<sup>1,D–F</sup>

<sup>1</sup> Department of Nephrology and Transplantation Medicine, Wrocław Medical University, Poland

<sup>2</sup> Department of Nephrology and Transplantation Medicine, University Clinical Hospital, Wrocław, Poland

A – research concept and design; B – collection and/or assembly of data; C – data analysis and interpretation;

D – writing the article; E – critical revision of the article; F – final approval of the article

Polymers in Medicine, ISSN 0370-0747 (print), ISSN 2451-2699 (online)

*Polim Med.* 2019;49(2):67–70

## Address for correspondence

Maciej Szymczak

E-mail: maciej.szymczak@umed.wroc.pl

## Funding sources

None declared

## Conflict of interest

None declared

Received on February 5, 2020

Reviewed on April 25, 2020

Accepted on May 4, 2020

## Abstract

Free light chains accumulation is the reason of kidney injury in patients with multiple myeloma. The removal of free light chains can improve patients prognosis and survival, and in some cases allows for dialysotherapy discontinuation. Unfortunately, conventional dialysis is not effective enough in terms of free light chains removal. New high cut-off (HCO) techniques remove free light chains more effectively than conventional dialysis. In some cases, this technique may turn out better than hemodiafiltration. However, there are some differences between specific techniques in the removal of kappa and lambda light chains. Lambda light chains are better removed by polymethyl methacrylate membranes with a change of filter during dialysis. Kappa light chains are thoroughly removed by polymethyl methacrylate membranes and HCO (35,000 Da) polysulfone membranes. Unfortunately, it is very difficult to differentiate between the effect of HCO dialysis therapy and concomitant chemotherapy because some of the data is not fully conclusive. Using the proper technique for an individual patient may give optimally effective treatment results.

**Key words:** treatment, multiple myeloma, dialysis membranes

## Cite as

Szymczak M, Zielińska D, Musiała A. The use of different dialysis membranes in therapy of patients with multiple myeloma.

*Polim Med.* 2019;49(2):67–70. doi:10.17219/pim/122014

## DOI

10.17219/pim/122014

## Copyright

© 2020 by Wrocław Medical University

This is an article distributed under the terms of the

Creative Commons Attribution 3.0 Unported (CC BY 3.0)

(<https://creativecommons.org/licenses/by/3.0/>)

## Introduction

Conventional hemodialysis is unable to remove effectively the circulating free light chains in patients with multiple myeloma (MM). New high cut-off (HCO) dialysis techniques make it possible to decrease levels/concentrations of free light chains, especially with simultaneous chemotherapy treatment. Hemodiafiltration with ultrafiltrate regeneration on resin using 'super-high-flux' (polyphenylene super-high-flux (S-HF), with a nominal cut-off of 42 kD) membrane also effectively decreases free light chains concentrations. This kind of hemodiafiltration does not have any influence on albumin concentration.<sup>1</sup> Using HCO membranes allows for stopping dialysis in some patients with MM (3 out of 5 in this study).<sup>2</sup>

Utilizing HCO membranes was associated with a higher rate of hemodialysis independence at 6 months (56.5% HCO hemodialysis vs 35.4% conventional hemodialysis) and 12 months (60.9% HCO hemodialysis vs 37.5% conventional hemodialysis). The frequency of adverse effects was similar in both groups (43% of complications connected with hemodialysis in the HCO group in comparison to 39% in the conventional group), and mortality was similar in both groups.<sup>3</sup>

Similar results were achieved in terms of dialysis independence after 6 and 9 months of treatment when HCO dialysis membranes with bortezomib were used – 6 out of 10 patients no longer needed dialysis, compared to 2 out of 10 patients undergoing conventional dialysis with bortezomib.<sup>4</sup>

Other authors found that in patients with MM, using HCO membranes results in lower mortality in comparison to conventional membranes. The survival rate after 1 year of treatment was 25% in the group of patients dialyzed using HCO dialyzer compared to 0% when a conventional dialysis was performed. Complete renal response rate, defined as an increase from <50 mL/min to >60 mL/min for at least 2 months, was 10.5% among patients treated with HCO dialyzers compared to 0% among patients treated with conventional dialysis. Partial renal response rate, defined as an increase of estimated glomerular filtration rate (eGFR) from <15 mL/min to 30–59 mL/min, was 15.8% and 5.3% in HCO dialysis- and conventional dialysis-treated patients, respectively, while minor renal response rate, defined as an increase from <15 mL/min to 15–29 mL/min or from 15–29 mL/min to 30–59 mL/min, was 26.3% and 15.8% in HCO dialysis- and conventional dialysis-treated patients, respectively. Increased survival rate of patients and renal response rate correlated with a decrease of free light chains concentration. Total treatment costs were comparable in both groups of patients treated with usage of HCO membranes and conventional dialysis.<sup>5</sup> While HCO membranes are more expensive than conventional ones, better overall treatment results lead to decreased total treatment costs, offsetting the higher price of HCO membranes.<sup>6</sup>

## Polymethylmethacrylate membranes

The use of adsorptive membranes, such as polymethylmethacrylate-based BK-2.1 membrane, was also associated with better outcomes among patients with myeloma and cast nephropathy.<sup>7</sup>

Combining Theralite 2100 SUPRA device (Bellco, Mirandola, Italy), bortezomib and dexamethasone treatment resulted in a decrease of free light chains concentrations ranging from 72.8% to 99.7% in 3 weeks. Response to treatment was achieved in 80% of patients with acute kidney injury in the course of MM.<sup>8</sup>

High cut-off membranes dialysis effectively diminished free light chains concentrations in patients with acute kidney injury. A total of 11.6 six-hour HCO dialysis sessions per patient were performed, with free light chains decreasing by 93.7% in the course of treatment. Single dialysis session decreased free light chains by about 57.7%.<sup>9</sup>

On the other hand, a comparison of dialysis using polymethyl methacrylate membranes (PMMA), one of the most common HCO dialysis membranes, with conventional dialysis for patients simultaneously treated with bortezomib indicate no differences between these modalities after 3 months of treatment. The results of treatment were dependent on the hematologic response for treatment (56% of patients with hematological response and 6.7% of patients without hematologic response were independent from dialysis).<sup>10</sup>

## Double polymethacrylate membranes

Nonetheless, it was proved that the double polymethylmethacrylate filter (DELETE system) (Toray BK-F; Toray Industries, Inc., Tokyo, Japan) was effective in terms of free light chain removal in chronic dialysis patients with MM.<sup>11</sup>

Exchange of PMMA filter after 2 h of dialysis increased lambda light chains removal rates compared to classic PMMA, as it mitigated rapid PMMA saturation with free lambda chains, which diminishes their efficacy in removing the lambda chains. This kind of dialysis is called enhanced adsorption dialysis (EAD). The reason of this phenomenon is fast PMMA saturation with free lambda chains. Saturation of PMMA with free light chains decreases free lambda light chains removal efficacy.

This phenomenon was not observed in kappa light chains removal. It is suggested that the EAD method may be important in the treatment of MM patients with high concentrations of lambda light chains.<sup>12</sup> High cut-off PMMA dialysis removes free light chains mainly through adsorption. In the course of hemodiafiltration, more free light chains are removed than in the used dialysis solution. High cut-off PMMA removes kappa light chains more effectively than hemodiafiltration.<sup>13</sup>

## Other membranes

More effective clearance of kappa light chains compared to lambda light chains was observed also in 24 h dialysis using a HCO (35,000 Da) polysulfone membrane.<sup>14</sup> Light chains appear not only in MM; they are classified as free medium urea toxins. Comparison of free dialysis membranes: PMMA, polyphenylene HFR17 filter and conventional polysulfone filter F7HPS in terms of kappa and lambda free light chains removal indicates that PMMA and polyphenylene HFR17 filter are more effective than conventional polysulfone filter F7HPS.<sup>15</sup>

## Efficacy control

It should be taken into account that dialysis membranes with nominally the same parameters may have a different efficacy of clearance.<sup>16</sup> The structure of monoclonal protein is different in every patient and the real efficacy of free light chains should be controlled. Free light chains concentration should be checked every week of dialysis treatment.<sup>15</sup> Actually, published data indicates that better prognosis is correlated with the extent of free light chain reduction in serum.<sup>5</sup>

## Controversies

Contrary to the data indicating the superiority of HCO hemodialysis over conventional dialyzers, there are 2 multicenter randomized controlled trials in which this superiority was not confirmed. In MYRE study (98 participants and 48 hospitals in France), no statistically significant difference was shown in the hemodialysis independence rate between patients treated with HCO compared to conventional hemodialysis for 3 months (41.3% and 33%, respectively,  $p = 0.42$ ), although a significantly higher clearance of light chains in HCO dialyzers group was noticed.<sup>3</sup> Significant difference in hemodialysis independence appeared 6 and 12 months of treatment (56.5% vs 35.4% and 60.9% vs 37.5%, respectively) but, as the authors of MYRE study concluded, these results should be considered exploratory. In EuLITE study (90 patients and 16 hospitals in UK and Germany), hemodialysis independence was observed in 56% of patients treated with HCO dialyzers and in 51% patients in the standard hemodialysis group ( $p = 0.81$ ). More infections were observed as adverse events in HCO hemodialysis group, including lung infections (26 vs 13 infections, 14 vs 3 lung infections).<sup>17</sup>

## Summary

The efficacy of HCO dialysis membranes in terms of diminishing free light chains resulted in guidelines of the International Myeloma Working Group Recommendations

for the Diagnosis and Management of Myeloma-Related Renal Impairment: The use of HCO dialyzers in combination with anti-myeloma therapy should be considered (grade B).<sup>18</sup> The use of HCO dialyzers in combination with anti-myeloma therapy seems to be a good option for treating patients with MM. However, future studies should precise the indications for this therapy.

### ORCID iDs

Maciej Szymczak  <https://orcid.org/0000-0002-1248-081X>  
Dorota Zielińska  <https://orcid.org/0000-0003-1861-2622>  
Aleksandra Musiała  <https://orcid.org/0000-0001-7358-2046>

### References

- Menè P, Giammariolia E, Fofia C, et al. Serum free light chains removal by HFR hemodiafiltration in patients with multiple myeloma and acute kidney injury: A case series. *Kidney Blood Press Res.* 2018;43(4):1263–1272.
- Peters NO, Laurain E, Cridlig J, Hulin C, Cao-Huu T, Frimat L. Impact of free light chain hemodialysis in myeloma cast nephropathy: A case-control study. *Hemodial Int.* 2011;15(4):538–545.
- Bridoux F, Carron PL, Pegourie B, et al; MYRE Study Group. Effect of high-cutoff hemodialysis vs conventional hemodialysis on hemodialysis independence among patients with myeloma cast nephropathy: A randomized clinical trial. *JAMA.* 2017;318(21):2099–2110.
- Buus NH, Rantanen JM, Krag SP, Andersen NF, Jensen JD. Hemodialysis using high cut off filters in light chain cast nephropathy. *Blood Purif.* 2015;40(3):223–231.
- Curti A, Schwarz A, Trachsler J, Tomonaga Y, Ambühl PM. Therapeutic efficacy and cost effectiveness of high cut-off dialyzers compared to conventional dialysis in patients with cast nephropathy. *PLoS One.* 2016;11(7):e0159942. doi:10.1371/journal.pone.0159942
- Florens N, Juillard L. Expanded haemodialysis: News from the field. *Nephrol Dial Transplant.* 2018;33(Suppl 3):iii48–iii52.
- Sens F, Chaintreuil D, Jolivot A, et al. Effectiveness of IHD with adsorptive PMMA membrane in myeloma cast nephropathy: A cohort study. *Am J Nephrol.* 2017;46(5):355–363.
- Buti E, Dervishi E, Ghiandai G, et al. Free light chains reduction on acute kidney injury in multiple myeloma: Critical role of high cut-off membranes [In Italian]. *G Ital Nefrol.* 2014;31(6):gin/31.6.11.
- Berni Wennekers A, Martin Azara MP, Dourdil Sahun V, et al. Thirteen treated of acute renal failure secondary to multiple myeloma with high cut off filters. *Nefrologia.* 2016;36(4):418–426.
- Hudier L, Decaux O, Haddj-Elmabet A, et al. Intensive haemodialysis using PMMA dialyser does not increase renal response rate in multiple myeloma patients with acute kidney injury. *Clin Kidney J.* 2018;11(2):230–235.
- Santoro A, Grazia M, Mancini E. The double polymethylmethacrylate filter (DELETE system) in the removal of light chains in chronic dialysis patients with multiple myeloma. *Blood Purif.* 2013;35(Suppl 2):5–13.
- Fabbrini P, Sirtori S, Casiraghi E, et al. Polymethylmethacrylate membrane and serum free light chain removal: Enhancing adsorption properties. *Blood Purif.* 2013;35(Suppl 2):52–58.
- Oshihara W, Nagao H, Megano H, Arai J, Koide M, Takada M. Trial use of a polymethylmethacrylate membrane for the removal of free immunoglobulin light chains in dialysis patients. *NDT Plus.* 2010;3(Suppl 1):i3–i7.
- Hanf W, Guillaume C, Jolivot A, et al. Prolonged hemodialysis for acute kidney injury in myeloma patients. *Clin Nephrol.* 2010;74(4):319–322.
- Donati G, Moretti MI, Baraldi O, et al. Removal of free light chains in hemodialysis patients without multiple myeloma: A crossover comparison of three different dialyzers. *BMC Nephrol.* 2016;17(1):193.
- Ouseph R, Hutchison CA, Ward RA. Differences in solute removal by two high-flux membranes of nominally similar synthetic polymers. *Nephrol Dial Transplant.* 2008;23(5):1704–1712.

17. Hutchison CA, Cockwell P, Moroz V, et al. High cutoff versus high-flux haemodialysis for myeloma cast nephropathy in patients receiving bortezomib-based chemotherapy (EuLITE): A phase 2 randomised controlled trial. *Lancet Haematol.* 2019;6(4):e217–e228.
18. Dimopoulos MA, Sonneveld P, Leung N, et al. International Myeloma Working Group Recommendations for the Diagnosis and Management of Myeloma-Related Renal Impairment. *J Clin Oncol.* 2016;34(13):1544–1557.

# Comprehensive review of the role of acrylic acid derivative polymers in floating drug delivery system

Beena Kumari<sup>1,2,A–C</sup>, Aparna Khansili<sup>2,B,D–E</sup>, Parmita Phougat<sup>3,B,D</sup>, Manish Kumar<sup>4,D,F</sup>

<sup>1</sup> Department of Pharmaceutical Sciences, Indira Gandhi University, Rewari, India

<sup>2</sup> Department of Pharmacy, School of Medical and Allied Sciences, GD Goenka University, Gurugram, India

<sup>3</sup> Pandit Bhagwat Dayal Sharma Post Graduate Institute of Medical Sciences, Rohtak, India

<sup>4</sup> MM College of Pharmacy, Maharishi Markandeshwar (Deemed to be University), Mullana-Ambala, India

A – research concept and design; B – collection and/or assembly of data; C – data analysis and interpretation;

D – writing the article; E – critical revision of the article; F – final approval of the article

Polymers in Medicine, ISSN 0370-0747 (print), ISSN 2451-2699 (online)

*Polim Med.* 2019;49(2):71–79

## Address for correspondence

Manish Kumar

E-mail: manish\_singh17@rediffmail.com

## Funding sources

None declared

## Conflict of interest

None declared

Received on January 28, 2020

Reviewed on March 31, 2020

Accepted on May 4, 2020

## Abstract

In the development of drug delivery systems, an oral drug delivery system is the preferred route of drug administration. Many components play an important role in developing a drug delivery system. Amongst those components, polymers have evolved with these systems. Macromolecule compounds consisting of many monomer units which are joined to each other by different bonds are known as polymers. For drugs that are absorbed primarily in the upper gastrointestinal tract, floating drug delivery systems offer an additional advantage. The purpose behind this review was to focus on different types of floating drug delivery systems and different types of polymers used in floating drug delivery systems, focusing on acrylic acid derivatives and their applications. In this review, the main emphasis is on acrylic acid derivative polymers, their formulation and grades, and various patents on these types of polymers. Based on the literature survey, mainly 2 types of polymers are used in this drug delivery system; i.e., natural and synthetic. Examples of natural polymers are xanthan gum, guar gum or chitosan, and synthetic polymers include acrylic acid derivatives and hydroxypropyl methylcellulose (HPMC). Eudragit and Carbopol are the most widely used acrylic acid derivatives.

**Key words:** acrylic polymers, Eudragit, floating drug delivery system, acrylic acid derivatives, carbomer

## Cite as

Kumari B, Khansili A, Phougat P, Manish Kumar M. Comprehensive review of the role of acrylic acid derivative polymers in floating drug delivery system. *Polim Med.* 2019;49(2):71–79. doi:10.17219/pim/122016

## DOI

10.17219/pim/122016

## Copyright

© 2020 by Wrocław Medical University

This is an article distributed under the terms of the Creative Commons Attribution 3.0 Unported (CC BY 3.0)

(<https://creativecommons.org/licenses/by/3.0/>)

## Introduction

A gastro-retentive drug delivery system (floating), which is less dense than gastric fluids, thus remaining buoyant in the stomach for a prolonged period, and which does not affect the gastric emptying rate is known as a floating drug delivery system (FDDS).<sup>1</sup> Floating drug delivery systems are also known as hydro-dynamically balanced systems (HBS). The system floats within the gastric contents and the drug is released at the desired rate from the system.<sup>2,3</sup> The remainder of the system is emptied from the stomach after the release of the drug; as a result, an increased gastric residence time (GRT) and a better control of fluctuations in plasma drug concentration can be achieved. The differences between zero-order controlled release and sustained release are shown in Fig. 1.

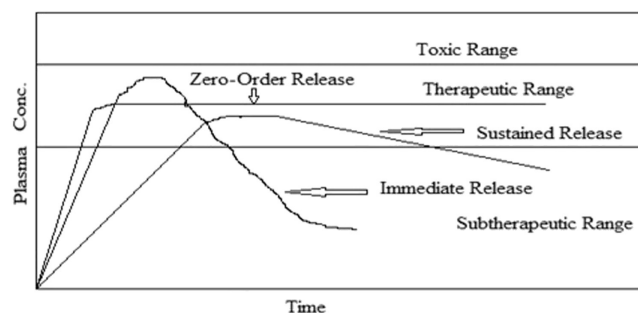


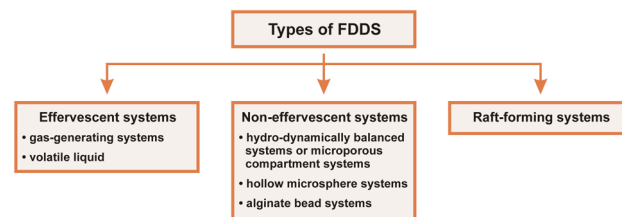
Fig. 1. Drug release profile, showing the differences between zero-order controlled and sustained release

## Types of floating drug delivery systems

There are various types of commercially available FDDSs<sup>4,5</sup> through which drugs are administered to the body and the effective controlled release of a drug is achieved. Some of these formulations are described in Table 1.<sup>6</sup>

Table 1. Commercially available floating formulations

Name of the product	Active ingredient	Category	Remarks
Madopar	levodopa and benserazide	anti-parkinsonian	floating, controlled-release (cr)
Valrelease	diazepam	anti-anxiety	floating capsule
Gaviscon	Al hydroxide Mg carbonate	antacid (in reflux esophagitis)	effervescent floating liquid alginate preparation
Cytotec	misoprostol	antiulcer	floating dosage form
Topalkan	alginic acid, aluminium and magnesium salts	antacid	floating liquid alginate preparation
Almagate flowcoat	Al-Mg antacid	antacid	floating dosage form



## Polymers used in floating drug delivery systems

In a floating drug delivery system, many polymers are used to target drug delivery at a specific region within the stomach. Both types of polymers, i.e., synthetic and natural, are used in such a system. Natural polymers like chitosan, xanthan gum and sodium alginate are used in a floating system, while synthetic polymers, such as hydroxylpropyl methylcellulose (HPMC), ethyl cellulose and acrylic acid derivatives, are used for the floating drug delivery.<sup>7</sup> Different natural and synthetic polymers and their properties are listed in Table 2.

Natural polymers have some inherent disadvantages, such as microbial contamination, variation between batches, uncontrolled hydration rate, and loss of viscosity in storage.<sup>8</sup>

## Synthetic polymers

Synthetic polymers are macromolecules with very large chains containing a variety of functional groups. They have a very wide range of uses, and are thus becoming more and more important in pharmaceuticals. The uses of synthetic polymers, e.g., as a binder or film coating agent for targeted drug delivery, are very common. Synthetic polymers are either purely synthetic or semi-synthetic, the latter being a modified form of natural polymers.<sup>9</sup>

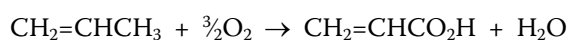
Some examples of synthetic polymers are Eudragit or Carbopol, which are acrylic acid derivatives, and HPMC.

Table 2. List of polymers and their properties

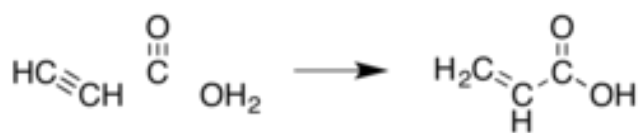
No.	Polymer (type)	Source	Properties
1.	guar gum (natural)	endosperm of seed of cynopsis tetragonolobus	insoluble in organic solvents, strong hydrogen bond
2.	chitosan (natural)	shell of marine invertebrates	nontoxic, biodegradable, biocompatible
3.	xanthan gum (natural)	fermentation of glucose by <i>Xanthomonas campestris</i>	excellent solubility and stability under acidic and alkaline conditions
4.	gellan gum (natural)	<i>Pseudomonas elodea</i>	high gel strength, an excellent stability, process flexibility, high clarity
5.	sodium alginate (natural)	<i>Laminaria hyperborica</i>	acidity/alkalinity pH-7.2 (1% w/v aqueous solution)
6.	Eudragit (synthetic)	acrylamide monomer	Eudragit S and FS are soluble at pH above 7 while Eudragit L is soluble at pH above 6. Eudragit RL, NE 40D, RS, NE 30D, and NM 30D are used to form water-insoluble film coats.
7.	ethyl cellulose (synthetic)	prepared from cellulose, it is a partly O-ethylated cellulose, its ethoxy content (-OC <sub>2</sub> H <sub>5</sub> ) is 44–51%	water-insoluble cellulose ether

## Acrylic acid

Byproduct of the production of ethylene and gasoline, acrylic acid is produced by the oxidation of propylene:



The IUPAC name of acrylic acid is propenoic acid. It is an organic compound with the formula CH<sub>2</sub>=CHCOOH. It has good solubility with water, ethers, chloroform, and alcohols.<sup>10</sup>



## Acrylic acid derivatives

There are many derivatives for the preparation of floating microspheres to be used as polymers. Of these numerous polymers, Eudragit and Carbopol are the most commonly used derivatives. A derivative of acrylic and methacrylic acids, such as Eudragit and its various grades – RL, E and RS – are used in the preparation of floating microspheres.<sup>10</sup> The grades RL 100 and RS 100 are both granular in nature and are the most widely used forms of any pH-independent swelling polymer with muco/adhesive properties.<sup>11</sup>

For sustained-release products and to form water-insoluble film coatings, Eudragit RL, NM 30D, NE 30D, RS, and NE 40D are used. Varying permeability films can be obtained by mixing any 2 polymers, but Eudragit RL films are more permeable than Eudragit RS. In aqueous as well as organic wet-granulation processes, polymethacrylates

are also used as binders. To control the release of a drug from a tablet matrix, more (5–20%) dry polymer is used; solid polymers (10–50%) may be used in direct compression processes. To prepare novel gel formulations for rectal delivery and the matrix layers of transdermal delivery systems, polymethacrylate polymers are also used.<sup>12</sup>

## History of Eudragit

Before the 19<sup>th</sup> century, the control of drug release time and its release site was impossible. In order to remove this main drawback, scientists can use polymers to plan and modulate the release of drug. The discovery of Eudragit by Rohm and Haas played a major role in finding the solution to this problem. Over time, various grades of Eudragit have been discovered, with varying degrees of solubility. To coat solid drugs, as with tablets, capsules or granular formulations, Eudragit is used as an excipient. Then, in the 1950s, the use of Eudragit in drug release was first discovered when a coated pill that dissolves in stomach acid was released. Since then, many other variants of Eudragit which control the drug release time have become available, but these are called retard preparations because they release their drugs at intestinal pH due to their resistance to stomach pH.<sup>13</sup> Eudragit is a trademark of Rohm GmbH and Co. KG. Eudragit is produced through the polymerization of acrylic and methacrylic acids or their esters, such as butyl ester.<sup>14</sup> The different grades of Eudragit are introduced in chronological order in Table 3.

## Glass transition temperature

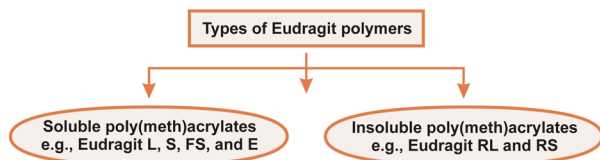
In the description of the physical properties of polymers, glass transition temperature is an important factor. The solidification of an anisotropic polymer melt is

**Table 3.** Specifications and applications of different grades of Eudragit

Grade of Eudragit	Year of introduction	Available form	Glass transition temperatures (T <sub>g</sub> )	Dissolution properties	Applications
RL 100	1968	granules	63	insoluble	sustained release
RL 30 D	1986	30% aqueous dispersion	55	pH-independent	sustained release
RS 100	1968	granules	65	insoluble	sustained release
RL 12.5	1954	12.5% organic solution	130 (±5)	–	sustained release
RL PO	1972	powder	63	high permeability	sustained release
RS 12.5	1954	12.5% organic solution	130 (±5)	–	sustained release
RS PO	1972	powder	65	low permeability	film coating
NE 40 D	1983	40% aqueous dispersion	–8	pH-independent swelling	film coating
RS 30 D	1986	30% aqueous dispersion	55	pH-independent swelling	sustained release
NE 30 D 30 %	1972	aqueous dispersion	–8	Insoluble, low permeability	film coating

described on a macroscopic level. In short, as the temperature is increased, the glass transition or glass–liquid transition is the reversible change in an amorphous product from a solid and moderately brittle “glassy” state into a rubbery or viscous state.<sup>15</sup> The glass transition temperature of different grades of Eudragit is presented in Table 3.

## Types of Eudragit polymers



### 1. Soluble poly(meth)acrylates

Soluble poly(meth)acrylates will dissolve in digestive fluids by forming salt and are able to release a drug at certain pH levels with acidic or alkaline groups.

#### Applications

Through simple masking and gastric resistance, the drug is delivered to all sections of the intestine for controlled drug release.

### 2. Insoluble poly(meth)acrylates

Insoluble poly(meth)acrylates are permeable in digestive fluids but insoluble in nature. For example, by pH-independent swelling Eudragit RL and RS polymers are able to control the drug release time in alkaline conditions, while Eudragit NE polymers are able to do so with neutral groups.

## Advantages of Eudragit polymers

The advantages of the acrylic acid derivative<sup>16</sup> Eudragit are listed in Fig. 2.

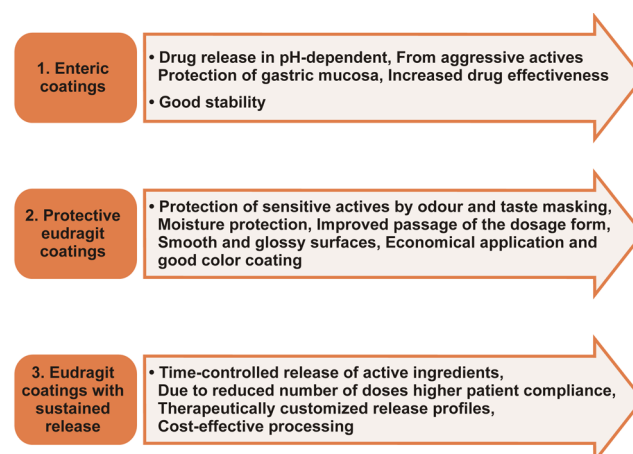


Fig. 2. Advantages of Eudragit polymers

## Carbopol

Another acrylic acid derivative with a high mucoadhesive property and a high swelling property is Carbopol; it is very often used in FDDSs. Carbopol is used alone and in combination with other polymers, such as Eudragit or natural polymers, in preparations of floating formulations.<sup>17–19</sup> By using the emulsification solvent evaporation method, floating microspheres can also be prepared with different grades of Carbopol: Carbopol 934, Carbopol 910, Carbopol 940, and Carbopol 941. The different grades of carbomer and their uses, viscosities and properties are described in Table 4. This floating system has been accepted as a process to accomplish controlled drug delivery by delaying the residence time of the dosage form at the site of absorption, thereby enhancing the bioavailability of the active ingredient.<sup>20–22</sup> The advantages of this polymer are summarized in Fig. 3.



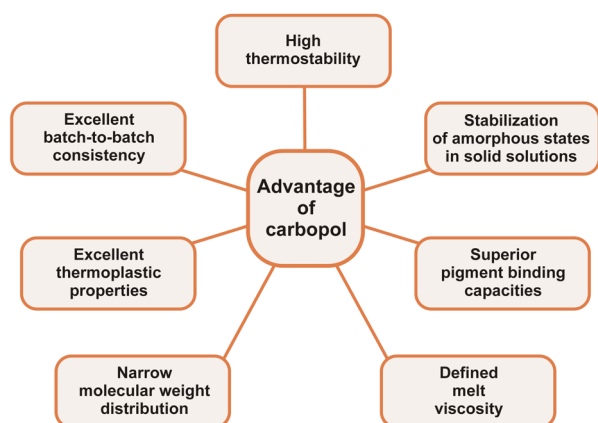


Fig. 3. Advantages of Carbopol polymers

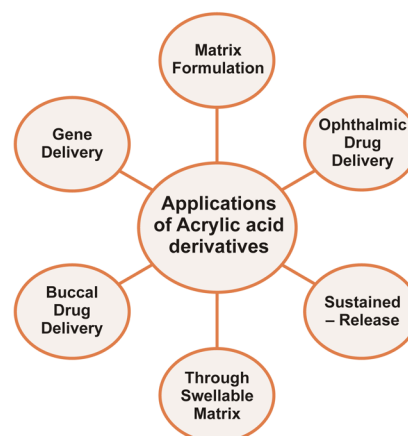


Fig. 4. The role of acrylic acid derivatives in drug delivery

## Pharmaceutical applications of acrylic acid derivatives

There are numerous applications of acrylic acid derivatives; they are primarily used as tablet coatings, film forming agents, tablet binders, etc. Eudragit E12.5 is a 12.5% solution in propanol acetone (60:40) with a molecular weight of 32,000 g/mol. It is available as an organic solution and is mainly used as a film coating agent. It appears light yellowish in color and is soluble at a pH of less than 5. It is miscible in ethyl acetate, acetone, alcohols, 1N HCl, dichloromethane, and petroleum ether.

Eudragit E100 is used for a targeted area such as the stomach. It is accessible as tinged granules which are colorless or yellow in color with an amine-like odor. Its properties include great pigment binding capacity, low polymer weight, low viscosity, and good adhesion. The solubility characteristics of Eudragit E100 are similar to Eudragit 12.5. Eudragit grade RSPO is available as a white powder and has a faint amine-like odor, while Eudragit RS 100 is available as a colorless granule with an odor similar to Eudragit RSPO.<sup>15</sup> The description and uses of Carbopol derivatives are presented in Table 4. The role of these polymers is depicted in Fig. 4.

Eudragit E PO is available as a free-flowing white powder which is used as a film coating agent. It is soluble in acetone and alcohols and in a pH of less than 5. Eudragit RS 100, RS 30D, RS 12.5, and RSPO are copolymers with quaternary ammonium groups of methyl methacrylate, ethyl acrylate and a small amount of methacrylic acid ester. The ammonium groups exist as salts and this permeability is an asset. Eudragit grade RS 30 D is available in liquid form. It has squat viscosity, a faint, characteristic odor, and a milky white color.<sup>15</sup> The widespread applications of different acrylic acid derivatives as single polymers or in combination with other natural or synthetic polymers are summarized in Table 5 along with their dosage form and method of preparation.

Different grades of Eudragit, such as RSPO, are available in powder form, while RS 30D, RS 100, and RS 12.5 are accessible in granular form, 30% aqueous dispersion and organic solution (12.5%), respectively; all grades are insoluble. They show pH-independent swelling with low permeability. Different grades of Eudragit are used in various ratios for the controlled and modified release profile.<sup>59</sup> Out of the many grades of Eudragit, a brief outline on RS 30D, RS 100 and RSPO is provided in Table 6.

Table 4. Different grades of carbomers and their properties

Name of polymer	Viscosity [Pa·s]	Used in dosage forms	Properties
Carbopol 910	3,000–7,000	emulgel, liposomal gel	Effective in low fixations and give a low consistency formulation.
Carbopol 940	40,000–60,000	emulgel	Effective in thick formulations and very great clarity in water or hydroalcoholic topical gels. Forms clear gels with hydroalcoholic frameworks.
Carbopol 941	4,000–11,000	emulgel	Produces low consistency gels and great clarity.
Carbopol 934	30,500–39,400	jojoba oil-based emulgel	Effective in thick details, for example, emulsions, suspensions, sustained release formulations, transdermals, and topicals. Forms clear gels with water.
Carbopol 934P	29,400–39,400	emulgel, liposomal gel	Same properties as 934; however, expected for pharmaceutical plans. "P" = exceptionally purified product

**Table 5.** List of drugs with their dosage form for gastric retention

Drug	Polymer	Dosage form	Method used	Reference
Ofloxacin	ethyl cellulose, sodium bicarbonate, Eudragit RL 30D	pellets	extrusion–spheronization	25
Itraconazole	chitosan	microspheres	ionotropic gelation	26
Norfloxacin	Eudragit®L100, Eudragit®RS 100	microballoons	emulsion solvent diffusion	27
Nifedipine	ethyl cellulose	microspheres	solvent evaporation	28
Bumetanide	Eudragit RS 100, sodium chloride, triethyl citrate	pellets	fluid bed layering and coating	29
Famotidine	Eudragit S 100	microspheres	solvent evaporation	30
Levodopa	gelatin, ethyl cellulose, carbidopa, L-poly(lactic acid), Eudragit S 100	novel unfolded CR-GRDF	solvent evaporation	31
Acacia catechu	Carbapol, HPMC and sodium CMC	microspheres	solvent evaporation	32
Pantaprazole	Eudragit L 100 and RS 100	microballoons	emulsion solvent diffusion	33
Piroxicam	alginate, pectin and HPMC	beads	ionotropic gelation method	34
Diclofenac potassium	Kollocoat SR 30D, Eudragit NE 30D and RS 30D	pellets	extrusion–spheronization	35
Carvedilol	chitosan	beads	ionotropic gelation method	36
Metformin hydrochloride	polyethylene oxide and Eudragit®L100	matrix tablets	direct compression	37
5- Fluorouracil	ethyl cellulose	microspheres	emulsion solvent diffusion	38
Levodopa	Eudragit®RL 30D, acetyl, triethyl citrate	floating coated mini-tabs	melt granulation and compression	39
Procyanidins	chitosan	capsules containing beads	ionotropic gelation method	40
Riboflavin	Eudragit L and Eudragit S plasticized with triethyl citrate	unfolding dosage form	accordion pill technology	41
Anthocyanin	calcium alginate, calcium carbonate, sodium acetate anhydrous and calcium chloride	microspheres	ionotropic gelation method	42
Diltiazem hydrochloride	sodium alginate, CaCO <sub>3</sub> , CaCl <sub>2</sub> , Eudragit RS 30D, and chitosan	floating microspheres	ionotropic gelation method	43
Clarithromycin	ethyl cellulose and HPMC E5	microspheres	solvent evaporation	44
Rabeprazole sodium	MC, Mannitol SD 200, Colorcoat EC4S, Kollidon CL	enteric coated tablet	wet granulation and direct compression	45
Nizatidine	Eudragit S 100 and HPMC	microballoons	emulsion solvent diffusion	46
Riboflavin	Eudragit RS 100 and HPMC	microballoons	emulsion solvent diffusion	47
Metformin	HPMC K4M, ethyl cellulose	microballoons	solvent evaporation	48
Ketoprofen floating	Eudragit S 100 and RL 100	microparticles	emulsion solvent diffusion	49
Medizide HCL	HPMC K 15M, Eudragit S 100 and RS 100	microspheres	solvent evaporation	50
Riboflavin	Eudragit S 100, PVA, dichloromethane, HPMC, and ethanol	microballoons	emulsion solvent diffusion	51
Repaglinide	PC, PPG	microspheres	solvent evaporation	52
Verapamil	Povidone K 30, talc, Eudragit NE 30 D and L 30 D, triethyl citrate	floating pellets	wet granulation and spheronization	53
Curcumin	ethyl cellulose	microspheres	emulsion solvent diffusion	54
Felodipine	ethyl cellulose	hollow microspheres	emulsion solvent diffusion	55
Riboflavin	Eudragit RS 100 and HPMC	microballoons	emulsion solvent diffusion	56
Fluconazole	Carbopol 934	liposomal gel	simple gelation method	57
Ketoconazole	Carbopol 934 and 940	emulgel	simple gelation method	58

Recently, Carbopol- and Eudragit-based formulations were collected for various patents and it was observed that formulations prepared using both of these polymers have been patented for diversified uses. Some of the patented applications are listed in Table 7, e.g., for colonic drug delivery, enhanced stability, improved bioavailability, improved hardness, oral drug delivery, reaction of carbomers, prolonged drug release, etc.<sup>59</sup>

## Conclusions

Acrylic acid derivative polymers have made significant contributions to various formulations due to their unique properties. In this article, the role of Carbopol and Eudragit was observed as novel and useful polymers, which can become more important in the future. This comprehensive review of 78 references signi-

**Table 6.** Specifications of Eudragit RS 30D, RS 100 and RSPO

Drug name	Grade of Eudragit	Method of preparation	Dosage form	Significance	Reference
Oxymatrine	Eudragit RS 30D	extrusion/spheronization	pellets	sustained release of drug for 12 h	60
Stavudine	Eudragit RSPO	solvent evaporation method	microspheres	sustained release	61
Ketoprofen	Eudragit RS 30D	same as in reference 60	pellets	The initial drug release is minimized but the terminal drug release increased more significantly.	62
Lobenzarit disodium	Eudragit RSPO	direct compression	tablet	slow drug release	63
Ambroxol hydrochloride	Eudragit RS 30D	same as in reference 60	pellets	stable as well as sustained release formulation	64
Verapamil hydrochloride	Eudragit RS 100	wet granulation method	matrix tablets	Coating with Eudragit RS 100 polymer reduced initial drug release.	65
Diclofenac sodium	Eudragit RS 30D	roto agglomeration	pellets	extended drug release for 24 h	66
Terbinafine hydrochloride	Eudragit RS 100	nano precipitation method	nanoparticles as eye drop	improved ocular bioavailability	67
Alfuzosin hydrochloride	Eudragit RSPO	same as in reference 63	tablets	The drug release was prolonged for 20 h.	68
Clotrimazole	Eudragit RS 100	spray drying technique	tablets containing microspheres	controlled intravaginal drug release	69
Theophylline	Eudragit RSPO	rotary tablet press	microtablets	sustained release	70
Genistein	Eudragit RS 100	melt-emulsification technique	nanostructured lipid carrier	Corneal penetration increases 3.3-fold.	71

**Table 7.** Patents on applications for acrylic acid derivatives

Title of the patent	Invention	Patent No.	Reference
Zinc/pectin beads with a Eudragit coating for colonic delivery	The systems comprise pectin beads which are cross-linked with any divalent cation or zinc which are coated with Eudragit polymers.	US 20080124279	73
With enhanced mechanical properties modified release tablet formulations	For said pharmaceutical formulation Eudragit L00-55 is used which achieves a desired hardness.	US 2007010	74
Enhanced stabilization of misoprostol	Misoprostol was complexed with several grades of Eudragit, such as RS series, RL series, Eudragit S and L; the solid dispersions were stable and showed sustain release.	EP0896823	75
Preparation method for the carbomer	Reaction in a mixed solvent of ethyl acetate and n-hexane and cyclohexane.	201310453464.3	-
Ursodeoxycholic acid-synthetic hydroxycitric acid-eudragit hybrid, pharmaceutical composition and method for preparing the same	The ursodeoxycholic acid-synthetic hydroxycitric acid-eudragit hybrid was used for bitter-taste-blocking effect and with high solubility improved body absorption rate.	US 2012015 6263	76
Oral drug delivery formulations	One active substance and minimum 1 coat containing Eudragit E in order to manage pain the preparation may be used for releasing loading dose up to about 55% of a total dose.	US 20150250733	77
Preparation of carbomers	Carbomer portion of the reaction medium is water instead of organic solvent such that the process toward the preparation of non-toxic carbomer, development of green direction.	201410010540.8	-
Coated senna extract granules	With 20% sennosides obtained from Senna extract are granulated with Eudragit grade L 100 and then covered with Eudragit grade L 30 D 55.	Wo/2011/014976	78

fies the uses of various grades of Eudragit and Carbopol polymers, which are the most widely used acrylic acid derivatives. The various drugs, dosage forms, and methods used to prepare formulations based on them have been described with all necessary details. These details are sufficient for the reader to understand the basic role of acrylic acid derivatives in different formulations. Some patents are also discussed in order to describe the current status of these polymers. Therefore, researchers can use this review as a guide to develop drug delivery systems based on acrylic acid derivatives, i.e., using Eudragit or Carbopol.

### ORCID iDs

Beena Kumari  <https://orcid.org/0000-0002-6333-5081>  
 Aparna Khansili  <https://orcid.org/0000-0001-7471-4266>  
 Parmita Phougat  <https://orcid.org/0000-0002-8867-8793>  
 Manish Kumar  <https://orcid.org/0000-0003-2042-1243>

### References

1. Avinash Y, Kaushik A, Tiwari K, Gaur A. Role of excipients and polymeric advancements in preparation of floating drug delivery systems. *Int J Pharm Investig.* 2015;5(1):1–12.
2. Nayak AK, Maji R, Das B. Gastro-retentive drug delivery systems: A review. *Asian J Pharma Clin Res.* 2010;3(1):2–9.
3. Lee JH, Park TG, Choi HK. Development of oral drug delivery system using floating microspheres. *J Microencapsul.* 1999;16:715–729.

4. Bansal AK, Chawla G, Gupta P, Koradia V. Gastro-retention: A means to address regional variability in intestinal absorption. *Pharma Tech*. 2003;2(1):50–68.
5. Zubedi SS, Mohammed S. Floating tablets and its polymers. *J Drug Deliv Therapeutics*. 2018;8(5):16–24.
6. Jain SK, Jain NK, Agrawal GP. Gastro-retentive floating drug delivery: An overview. *Drug Deliv Technol*. 2005;5:7–15.
7. Kumar G. Natural polymers in the development of floating drug delivery systems: A review. *Int J Pharm Life Sci*. 2013;2(4):165–178.
8. Darekar D. An overview on natural gum and its pharmaceutical application. *Int J Uni Pharmacy Biosci*. 2013;2:535–547.
9. Darekar D, Gupta P. An overview on natural gum and its pharmaceutical application. *Int J Uni Pharmacy Biosci*. 2014; 2: 432–447.
10. Joshi M. Role of Eudragit in targeted drug delivery. *Int J Curr Pharm Res*. 2013;5:58–62.
11. Sonje A, Chandra A. Comprehensive review on eudragit polymers. *Int Res J Pharm*. 2013;4:71–74.
12. Rowe R, Paul S. *Pharmaceutical Press*. Handbook of Pharmaceutical Excipient. 6<sup>th</sup> ed., 2009.
13. Stam JJ, Vink J, Lecessies S, Bruijn JA, Bregman W. Topical tretinoin under occlusion on a typical naevi. *Melanoma Res*. 1988;8:539–548.
14. Rieger MM, Lachman & Lieberman HA, Kanig JL. The Theory and Practice of Industrial Pharmacy. 3<sup>rd</sup> ed. 1986.
15. Gupta P, Kumar M, Sachan N. An overview on polymethacrylate polymers in gastro-retentive dosage forms. *Open Pharmaceutical Sciences J*. 2015;2:31–42.
16. Joshi M. Role of eudragit in targeted drug delivery. *Int J Current Pharma Res*. 2013;5(2):202.
17. Rayehe TR, Zahra JA, Seyed AM. Formulation and evaluation of captopril floating matrix tablets based on gas formation. *Afr J Pharm Pharmacol*. 2013;6:2438–2444.
18. Padma PS, Vandana P, Nisha V, Kausalya J, Vaijayanthi V, Ravichandiran V. Formulation and evaluation of gastro-retentive floating tablets of atenolol. *J Pharm Res*. 2011;4:3709–3711.
19. Tripathi GK, Singh S, Nath G. Formulation and in-vitro evaluation of pH-sensitive oil entrapped polymeric blend amoxicillin beads for the eradication of *Helicobacter pylori*. *Iran J Pharm Res*. 2012;11:447–455.
20. Kumar S, Chand T. Formulation and development of floating and mucoadhesive microspheres of clarithromycin. *Pharm Innov J*. 2013;2:19–26.
21. Gangdharappa HV, Biswas S, Getyala A, Gupta V, Kumar PT. Development, in-vitro and in-vivo evaluation of novel floating hollow microspheres of Rosiglitazone Maleate. *Der Pharm Lett*. 2011;3:299–316.
22. Wang J, Cui F, Shi K, Yang L, Wang S, Zhang L. In vivo evaluation of a sustained-release multiple-unit floating system containing nitrendipine. *Asian J Pharm Sci*. 2008;3:1517.
23. Samala ML, Sridevi G. Role of polymers as gelling agents in the formulation of emulgels. *Polym Sci*. 2016;1:21–32.
24. Prusty A, Gupta BK. Role of chitosan and eudragit in polymer-based extended release matrix tablets: A review. *Int J Pharm Sci Res*. 2017;8(12):4973–4982.
25. Chein YW. *Novel Drug Delivery Systems*. 2<sup>nd</sup> ed. New York, NY: Marcel Dekker; 2009.
26. Gokbulut E, Vural I, Aşikoğlu ON. Floating drug delivery system of itraconazole: Formulation, in vitro and in vivo studies. *J Drug Delivery Sci Tech*. 2019;49:491–501.
27. Zhang C, Xu MA. Floating multiparticulate system for ofloxacin based on a multilayer structure: In vitro and in vivo evaluation. *Int J Pharm*. 2012;430:141–150.
28. Parida P, Mishra SC, Sahoo S, Behera A, Nayak BP. Development and characterization of ethyl cellulose based microsphere for sustained release of Nifedipine. *J Pharma Analysis*. 2016;6:341–344.
29. Chaturvedi AK, Verma A, Singh A, Kumar A. Formulation and characterization of microballoons of norfloxacin. *J Drug Deliv Therapeutics*. 2011;1(2):21–26.
30. Gupta R, Prajapati SK, Pattnaik S, Bhardwaj P. *Asian Pac J Trop Biomed*. 2014;4(9):729–735.
31. Ehab H, Myron CG, Ronald WM, Adel S. A study of the pharmacodynamics differences between immediate and extended release bumetanide formulation. *Int J Pharm*. 2003;267:129–140.
32. Khare B, Dubey N, Sharma A. Antilucer activity of controlled release formulation containing aqueous extract of acacia catechu wild on rodent models. *Int J Curr Pharm Res*. 2018;10(5):25–31.
33. Gupta P, Kumar M, Kaushik D. Pantoprazole sodium loaded microballoons for the systemic approach: In vitro and in vivo evaluation. *Adv Pharm Bull*. 2017;7(3):461–467.
34. Giulia A, Andrea C, Francesca S, Aldo P, Silvana M, Rita P. Polysaccharides based gastro-retentive system to sustain piroxicam release: Development and in vivo prolonged anti-inflammatory effect. *Biomac*. 2018;6:213–219.
35. Atyabi F, Sharma HL, Mohammad, HA, Fell JT. In vivo evaluation of a novel gastro-retentive formulation based on ion exchange resins. *J Control Release*. 1996;42:105–113.
36. Radhakrishnan P, Verma P, Jayachandran V, et al. In vitro and in vivo evaluation of gastro-retentive carvedilol loaded chitosan beads using Gastroplus TM. *Int J Biol Macromol*. 2017;10:1016.
37. Jijun F, Xiaoli W, Lishuang X, Jia M. Preparation and in vitro in vivo evaluation of double layer coated and matrix sustained release pellet formulations of Diclofenac Potassium. *Int J Pharm*. 2011;406:84–90.
38. Huang Yu, Yumeng Wei, Hongru Y, et al. A 5-fluorouracil-loaded floating gastro-retentive hollow microsphere: Development, pharmacokinetic in rabbits, and biodistribution in tumor-bearing mice. *Drug Des Devel Ther*. 2016;10:997–1008.
39. Colo G, Falchi S, Zambito Y. In vitro evaluation of a system for pH-controlled peroral delivery of metformin. *J Control Release*. 2002;80:119–128.
40. Chen R, Guo X, Liu X, Cui H, Wang R, Han J. Formulation and statistical optimization of gastric floating alginate/oil/chitosan capsules loading procyanidins: In vitro and in vivo evaluations. *Int J Biol Macromol*. 2017;108:219–229.
41. Goole J, Deleuze P, Vanderbist F, Amighi K. New levodopa sustained release floating mini tablets coated with insoluble acrylic polymer. *Eur J Pharm Sci*. 2008;68:310–318.
42. Giovana B, Celli, Amyl G, Marianne S. Development and evaluation of floating alginate microspheres for oral delivery of anthocyanins: A preliminary investigation. *Food Sci Nutr*. 2017;5(3):713–721.
43. Kagan L, Lapidot N, Afargan M, Kirmayer D. Gastro-retentive accordion pill: Enhancement of riboflavin bioavailability in humans. *J Control Release*. 2006;113:208–215.
44. Nashar NN, Donia AA, Mady OY, Maghraby GM. Formulation of clarithromycin floating microspheres for eradication of *Helicobacter pylori*. *J Drug Delivery Sci Tech*. 2017;10:101–106.
45. Ninan M, Xu L, Wang Q, Zhang X. Development and evaluation of new sustained-release floating microspheres. *Int J Pharm*. 2008;358:82–90.
46. Jain A, Pandey V, Ganeshpurkar A, Dubey N, Bansal D. Formulation and characterization of floating microballoons of Nizatidine for effective treatment of gastric ulcers in murine model. *Drug Deliv*. 2015;22(3):306–311.
47. Strubing, S, Metz H, Mader K. Characterization of poly (vinyl acetate) based floating matrix tablets. *J Control Release*. 2008;126:149–155.
48. Yadav A, Jain DK. Gastro-retentive microballoons of metformin: Formulation development and characterization. *J Adv Pharm Technol Res*. 2011;2(1):51–55.
49. Sato Y, Kawashima Y, Takeuchi H, Yamamoto H. In vivo evaluation of riboflavin-containing microballoons for controlled drug delivery system in healthy human volunteers. *J Control Release*. 2003;93:39–47.
50. Hussein RA, Abu Lila, Abdallah MH, Hamed EE, El-Ghamry. Design, in vitro/in vivo evaluation of melizine HCl-loaded floating microspheres targeting pregnancy related nausea and vomiting. *J Drug Delivery Sci Tech*. 2018;5:135–142.
51. El-Kamel AH, Sokar MS, Al-Gamal SS, Naggar VF. Preparation and evaluation of ketoprofen floating oral delivery system. *Int J Pharm*. 2001;220:13–21.
52. Kumaraswamy S, Thangasundaralingam SR, Sekar R, Jayakrishnan A. A floating-type dosage form of repaglinide in polycarbonate microspheres. *J Drug Delivery Sci Tech*. 2017;10:201–213.
53. Sato Y, Kawashima Y, Takeuchi H, Yamamoto H. In vitro and in vivo evaluation of riboflavin-containing microballoons for a floating controlled drug delivery system in healthy humans. *Int J Pharm*. 2004;275:97–107.
54. Chao Pi, Ji Yuan Yuan, Hao Liu, et al. In vitro and in vivo evaluation of curcumin loaded hollow microspheres prepared with ethyl cellulose and citric acid. *Biomac*. 2017;45:17–425.

55. Pi C, Feng T, Liang J, et al. Polymer blends used to develop felodipine loaded hollow microspheres for improved oral bioavailability. *Int J Biol Macromol*. 2018;112:1038–1047.
56. Sato Y, Kawashima Y, Takeuchi H, Yamamoto H. Physicochemical properties to determine the buoyancy of hollow microspheres (microballoons) prepared by the emulsion solvent diffusion method. *Eur J Pharm Biopharm*. 2003;55:297–304.
57. Jain SK, Awasthi AM, Jain NK, Agrawal GP. Calcium silicate based microspheres of repaglinide for gastro-retentive floating drug delivery: Preparation and in vitro characterization. *J Control Release*. 2005;107:300–309.
58. Kawashima Y, Niwa T, Takeuchi H, Hino T, Itoh Y. Hollow microspheres for use as a floating controlled drug delivery system in the stomach. *J Pharm Sci*. 1992;81:135–140.
59. Patra CN, Priya R, Swain S, et al. Pharmaceutical significance of Eudragit: A review. *Future J Pharm Sci*. 2017;2:789–796.
60. Piao H, Liu S. Development of an osmotically-driven pellet coated with acrylic copolymers (Eudragit® RS 30D) for the sustained release of oxymatrine, a freely water soluble drug used to treat stress ulcers (I): In vitro and in vivo evaluation in rabbits. *Drug Dev Ind Pharm*. 2013;39:1230–1237.
61. Sahoo SK, Dhal S, Mohapatro P, Behera BC, Barik BB. Effect of processing temperature on Eudragit RS PO microsphere characteristics in the solvent evaporation process. *Pharmazie*. 2007;62:638–639.
62. Kibria G, Roni MA, Absar MS, Jalil RU. Effect of plasticizer on release kinetics of diclofenac sodium pellets coated with Eudragit RS30D. *AAPS Pharm Sci Tech*. 2008;9:1240–1246.
63. Boza A, Caraballo I, Alvarez JF, Rabasco AM. Evaluation of Eudragit RS-PO and Ethocel 100 matrices for the controlled release of loperamide hydrochloride. *Drug Dev Ind Pharm*. 1999;25:229–233.
64. Kibria G, Islam KM, Jalil RU. Stability study of ambroxol hydrochloride sustained release pellets coated with acrylic polymer. *Pak J Pharm Sci*. 2009;22:36–43.
65. Mathur V, Nagpal K, Singh SK, Mishra DN. Comparative release profile of sustained release matrix tablets of verapamil HCl. *Int J Pharm Investig*. 2013;3:60–65.
66. Krejčová K, Rabisková M, Vetchý D, Tomásek V, Prokopová A. The effect of polymeric dispersion type on the release of diclofenac sodium from coated pellets. *Ceska Slov Farm*. 2007;56:190–199.
67. Tayel SA, El-Nabarawi MA, Tadros MI, Abd-Elsalam WH. Positively charged polymeric nanoparticle reservoirs of terbinafine hydrochloride: preclinical implications for controlled drug delivery in the aqueous humor of rabbits. *AAPS Pharm Sci Tech*. 2013;14:782–793.
68. Roni MA, Kibria G, Jalil RF. Formulation and in vitro evaluation of alfuzosin extended release tablets using directly compressible eudragit. *Indian J Pharm Sci*. 2009;71:252–258.
69. Gupta NV, Natasha S, Getyala A, Bhat RS. Bioadhesive vaginal tablets containing spray dried microspheres loaded with clotrimazole for treatment of vaginal candidiasis. *Acta Pharm*. 2013;63:359–372.
70. Rey H, Wagner KG, Wehrle P, Schmidt PC. Development of matrix-based theophylline sustained-release microtablets. *Drug Dev Ind Pharm*. 2000;26:21–26.
71. Zhang W, Li X, Ye T, et al. Nanostructured lipid carrier surface modified with Eudragit RS 100 and its potential ophthalmic functions. *Int J Nanomed*. 2014;9:4305–4315.
72. Kibria G, Islam KM, Jalil RU. Stability study of ambroxol hydrochloride sustained release pellets coated with acrylic polymer. *Pak J Pharm Sci*. 2009;22:36–43.
73. Antoine A, Hélène, H. Colonic delivery using zn/pectin beads with a eudragit coating. US Patent: 20080124279. 2008.
74. Shojaei AH, Melissa EC. Modified release tablet formulations with enhanced mechanical properties. US Patent: 20070104782. 2007.
75. David C, Rong-jen T, Hue-in L. Improved stabilization of misoprostol. European Patent: 0896823. 2002.
76. Choy J, Choi GE, Park MC. Ursodeoxycholic acid-synthetic hydrocortisone Eudragit hybrid, pharmaceutical composition containing the same and method for preparing the same. US Patent: 20120156263. 2012.
77. Isa O. Oral drug delivery formulations. US Patent: 20150250733. 2015;September 10.
78. Jorge PH. Coated senna extract granules. WO/2011/014976. 2011; October 02.

Polimery w Medycynie  
Polymers in Medicine

